D. Geskus

Design and construction of regenerative amplifier and compressor for chirped pulse amplification

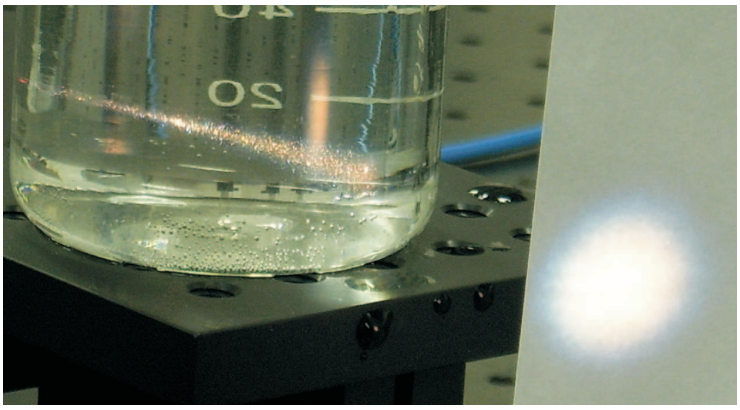

University of Twente
Enschede - The Netherlands

D. Geskus

Design and construction of regenerative amplifier and compressor for chirped pulse amplification

University of Twente
Department of Science and Technology
Laser Physics and Non-linear Optics
Enschede, July 11, 2006

Graduation Committee:
Prof. Dr. K.J. Boller
Dr. Ir. F.A. van Goor
Prof. Dr. M. Pollnau
Dr. H.J.W.M. Hoekstra

Summary

Research on acceleration of electrons by plasma waves will be performed at the laser physics and non-linear optics group of the University of Twente to develop a new compact method for acceleration of electrons. This method of electron acceleration requires an intense ultrashort laser pulse to induce a plasma wave in the plasma on which the electrons can "surf" to higher kinetic energies. Therefore, a laser is being developed that should deliver an 1 Joule laser pulse with a duration of 30 fs to generate the demanded 30 TW of optical power for creation of the plasma wave as required for this electron wake field acceleration experiment.
The principle of the laser is based on chirped pulse amplification; a stretched pulse is amplified to the demanded energy, and re-compressed afterwards.
This report describes the performed work concerning the design and construction of a pre-amplifier and a compressor. For pre-amplification of the pulse a regenerative amplifier is used, which has been constructed and characterised. The measured output power of the regenerative amplifier is approximately 3.5 mJ, in the future this pulse will be further amplified by two additional multi-pass amplifiers. But as this further amplification is beyond the scope of this master thesis, it will not be treated in this report. A grating compressor with an efficiency of approximately 70%, recompresses the pre-amplified pulse to a duration of 29 fs with a pulse energy of the compressed pulse of 2.5 mJ.
For creation of short pulses the dispersion of the optical system becomes very important. Because chirped pulse amplification is based on introducing dispersion in a controlled manner, it is of vital importance to fully comprehend these dispersive properties of the experimental set-up. Therefore, mathematical models have been successfully evaluated and the final output of the experimental set-up agrees very well to the results of the used mathematical models.

CONTENTS

Preface

The assignment of this masters thesis, was to design and construct a laser that generates an ultrashort laser pulse, and in case of sufficient available time, it would be an option to shoot the laser pulse at some material and measure the influences of this material on the properties of the pulse. But with experimental physics one has to rely on the used machines, in this case only three devices needed some unforeseen attention. It started with performing maintenance on the pump laser for the regenerative amplifier. After this laser had been serviced, the power supply of another pump laser started to generate errors. Fortunately this occurred not all the time, and did not cause large delay in the development of the experiment. After construction of the regenerative amplifier, the compressor had to be designed. During the construction of the compressor, it appeared that the grating surfaces were severely contaminated. After at least one month I succeeded to find a method to clean them again. During that month I started to characterise the output of the regenerative amplifier. These actions where aborted abruptly once the gratings were clean again and construction of the compressor could be started.
This introduction shows that the time balance of working with ultrashort laser techniques is not the most efficient one; after months of construction, the system operates for only a few femtoseconds. Fortunately this balance has been fully compensated by the nice atmosphere at the laser physics group. All the group members add their brick to this sphere, and I want to thank them all for being my colleagues. Some of these colleagues among them have to be mentioned more explicit, like Rolf Loch and Arie Irman, as I had many clarifying discussions about every day life and laser physics. And last but not least, I would like to thank Fred van Goor who patiently learned me how to treat delicate optics, and did not loose the confidence in my work, after peeling off the coating from one of the gratings.

Enschede, July 11, 2006

Dimitri Geskus

CHAPTER 1

Introduction

1.1 The laser physics group

The research of the laser physics group at the University of Twente is focussed on experiments using the special properties of laser light. Light produced by lasers can have many special properties like coherence, colour, intensity, and shape of pulse. Lasers, as we know them now, started their developments only 50 years ago. Though novel developments in the laser regime occur daily. This has enlarged the field of research enormously, so that now many research groups use lasers to perform their experiments. The laser physics group develops special lasers, in order to exploit their use in new regions of research. In this manner new theories can be proved, and fascinating non-linear effects can thus be demonstrated.

1.2 Acceleration of electrons

Particle accelerators are developed for use in many research fields. Still a large field has to be explored in this field of high energy physics, but progress is slow due to the costs of these machines. CERN for example has one giant accelerator, which is 27 km in circumference, making it a very expensive machine. These machines are that large, due to the fact that the particles have to be accelerated by an electric field. This field is generated with super conductive RF resonators and the maximum field that these machines nowadays can produce is 46 MV/m [1]. Acceleration of electrons with this type of accelerator to a modest energy of 20 GeV, requires an accelerator length of 20G/46M=435 meters. As this shows the reason for the large dimensions of these machines it is clear that we need stronger electric fields, in order to shrink the dimensions of these accelerators. A place where high electric fields can be found is in the core of atoms. A hydrogen atom for example has an electric field of $E = e/(4\pi\epsilon_0 a_0^2) \approx 5\ GVcm^{-1}$, where $e = 1.6 \cdot 10^{-19}$C (electron charge), $\epsilon_0 = 8.85 \cdot 10^{-12}\mathrm{Fm}^{-1}$ (electric permittivity of vacuum) and $a_0 = 5.29 \cdot 10^{-11}$m (Bohr radius). An accelerator with these electric fields would need only 4 centimetre to accelerate particles to energies

of 20 GeV. To access these fields a laser pulse is used to separate the electrons from the core. This can be performed in a plasma.

1.3 Plasma

Plasma is also called the fourth state of matter, besides solid, liquid and gas. In a plasma state the electrons are not bound to the residual core; the atoms of the material are ionised. There are many degrees of ionisation, and the easiest case is that of the hydrogen atom. When a hydrogen atom gets ionised, only one proton remains, and a free electron is created. When the matter is in complete plasma state all the atoms are completely ionised, creating a cloud of charged particles. The plasma has no nett charge, because the electrons and the atom cores are equally distributed due to electric interaction of the particles cancel out the electric fields. This balance of electron and ion density can be disturbed by a laser pulse. A strong laser pulse scatters the electrons in all directions due to so called ponderomotive forces, while as the position of the ions remains unchanged for a small time scale due to their larger masses. As a result a positive charged region remains. After the pulse has passed this region, the electrons will return to their original position driven by the generated electric field. Due to this implosion of the electrons an excess of electrons is generated after some time, so that the electrons will be scattered again, creating an oscillating potential field. As the laser pulse passes through the plasma, a potential wave will be created in the plasma, much like when one is walking through the wardrobe, and touching all the coat hangers when passing by. The result, shown in figure

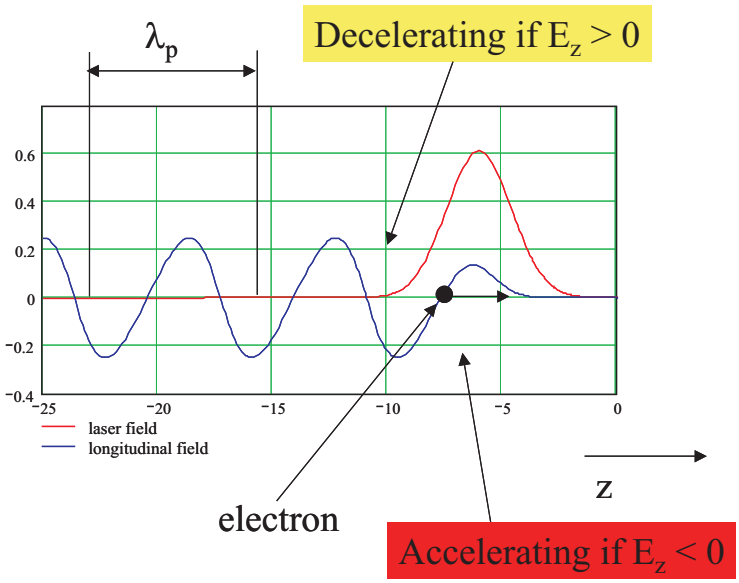

Figure 1.1: Plasma wakefield

1.1, is a travelling wave with a phase speed equal to the group velocity of the laser pulse. Injection of electrons at the right moment in this plasma wave with the same velocity of the laser pulse will let the electrons experience an electric

field in the propagation direction. This principle is better known as electron wake field acceleration. More details about plasma based particle accelerators can be found in [2].

1.4 University of Twente and the laser wake field acceleration demonstration experiment

In the laser wake field acceleration experiment, relativistic electrons will be further accelerated by a plasma wave which is induced by an ultra short laser pulse. Therefore it requires a harmonic symbioses of the following three physical aspects:

- Beam of relativistic electrons
- Ultra short, high energetic laser pulse, which is partly described in this report
- Plasma channel

It is an impossible task to develop these three fields simultaneous at a single institute. Therefore a collaboration between three institutes in the Netherlands share their expertises in this project. The cooperative institutes are:

- Laser Physics and Non-linear Optics group of the University of Twente, providing the 30 TW laser.
- FOM-Institute for Plasma Physics Rijnhuizen, Laser-Plasma XUV Source and XUV optics group, investing the plasma channel.
- Physics and Applications of Ion Beams and Accelerators group of the University of Eindhoven, providing the electron beam.

Together all the required physical aspects are covered, and each of the institutes has to develop their part to combine it into the project. But during the first years of this project things developed into different directions, and new ideas have been created at the University of Twente. These new ideas concern novel injection scheme of the electrons in the wake field [4] [5]. Now another project has started at the University of Twente. This parallel project concerns the construction of the complete experiment at the University of Twente. Fortunately the facilities of University of Twente cover all the demanded equipment for the experiment. An RF electron accelerator is leftover from a former free electron laser (FEL) project. The laser for the ultra short pulse is in any case under construction for the main project, only the plasma channel has to be developed from scratch. In the meanwhile the cooperation with the other institutes remains, not only for the initial project but also for the re-adjustments concerning the electron beam, and the development of the plasma channel. The demonstration experiment is still planned to be performed at the University of Eindhoven, but this is based on a different electron injection scheme [6].

CHAPTER 2

Laser system

Light intensities of several terawatts are required to perform electron wake field acceleration for the demonstration experiment at the University of Twente. The same intensities can be achieved by focussing all the sunlight that falls onto the earth onto the surface of a pinhead. These intensities are enormous and therefore it is not possible to generate this amount of light in a continuous manner, rather it has to be generated in a pulsed manner. The laser system used for this purpose

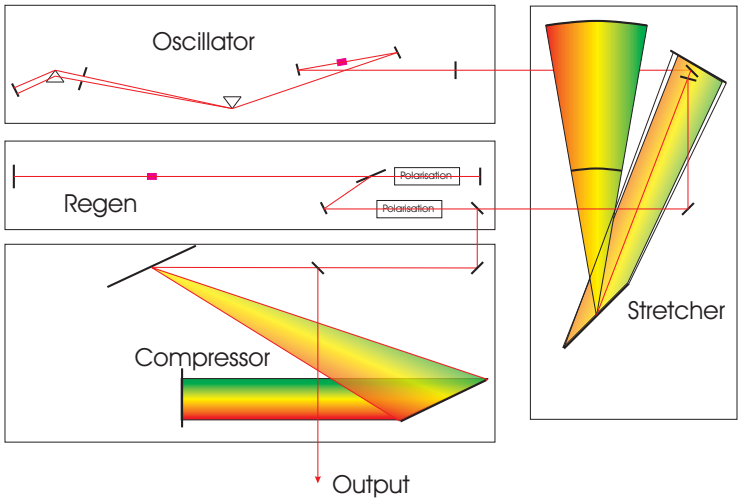

Figure 2.1: Chirped pulse amplification set up

is a combination of a Kerr-lens mode locked (KLM) laser in combination with a chirped pulse amplifier (CPA) system [3]. In this amplifier short pulses of a few femtoseconds from the KLM laser are stretched in time to a few hundreds of picoseconds, before they are amplified in three stages to two Joules of energy, at the end they are re-compressed to a few femtoseconds. After re-compression one Joule of pulse energy and 30 terawatt of optical power should be available, see figure 2.2. Two types of amplifiers are used in this system, a regenerative pre

amplifier and two multipass amplifiers. Further details concerning the choice of these types of amplifiers in this experiment is discussed in section 2.3. The

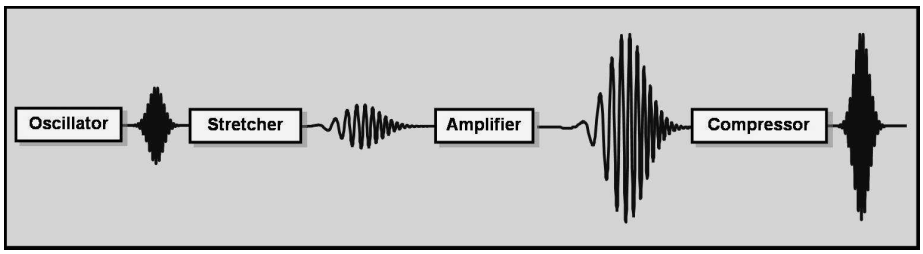

Figure 2.2: The pulse from the oscillator will be stretched, amplified and re-compressed to its original duration

following sections will describe the elements of the complete set up in sequence of the route that the initial pulse will travel through the set up.

2.1 Kerr lens modelocked laser

The initial pulse is generated in a KLM laser. This laser is based on a TiSa crystal, a material that is very suitable for generation and amplification of ultra short pulses, due to its very broad gain bandwidth of 235 nm around 800 nm [7]. The laser resonator, on the contrary, will not support this continuous spectrum, but only a limited number of discrete resonator modi. Resonator modi are introduced due to the resonator length (l), as most wavelengths will cancel themselves out by destructive interference after one or more cycles through the resonator cavity, as can been seen in figure 2.3. The frequency separation ($\triangle\nu$)

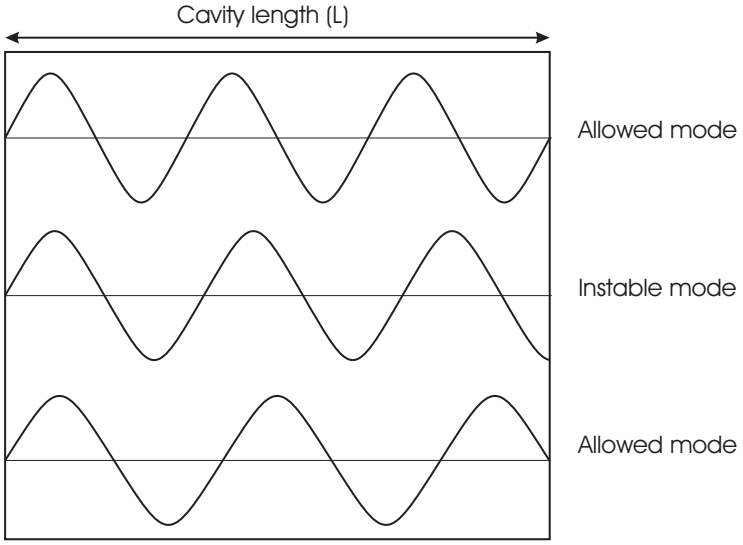

Figure 2.3: Cavity modi

between the successive modi is:

$$\triangle\nu = \frac{c}{2l}, \tag{2.1}$$

with c the velocity of light. Each individual longitudinal mode itself supports a small bandwidth, but typically this bandwidth is much smaller than the inter-mode frequency separation. Higher order transverse modi are suppressed by the geometry of the cavity. The combination of cavity length, concave mirrors and the apertures in the cavity will force the output to single transverse mode. A

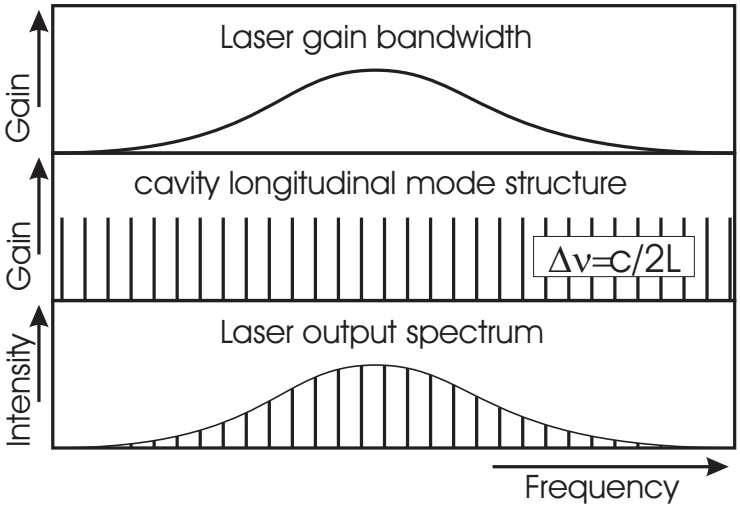

Figure 2.4: Laser spectrum

normal non-mode-locked laser will start to produce light in all of the supported laser modi, but after some roundtrips all energy will be concentrated into a few laser modi, namely those with the strongest gain. This reduces the bandwidth of the output light, which is of vital importance for generation of ultra short pulses. Therefore this effect has to be avoided. Mapping these modi onto the gain bandwidth of the TiSa crystal it is obvious that a large number of modi can be generated with this type of laser, shown in figure 2.4. To keep the laser from generating light in only a few of its modi, it should be operated in a pulsed mode. In a pulsed laser the modi with the strongest gain will less likely start to dominate the output of the laser, and the power is not concentrated in one frequency. To let the laser operate in an ultra short pulsed manner the modi have to be locked in a manner that all the modi involved have constructive interference at the same moment in time with each other. So in a modelocked laser all the modi are in phase with each other. The set up described here is based on Kerr lens mode locking, which is a passive modelocking technique. A Kerr-lens is made in material of which the refractive index n is strongly intensity dependent, according $n = n_0 + n_2 \cdot I$, with n_0 the low intensity refractive index, and n_2 the changes of the refractive index as function of the intensity of the light I. In the experimental set-up the TiSa crystal fulfils this role. When the intensity of the light is not sufficient no lens effect will occur in the material, but at higher intensities lensing effects will occur because the refractive index will be higher in centre of the laser pulse, creating a gradient index lens in the

material due to the spacial shape of the pulse. When a laser starts to operate in a pulsed mode, the energy will be compressed in time into pulses of high intensity. The average output power does not show large changes, as the pump energy remains unchanged. Then it is clear that the Kerr-effect will only occur when the laser is operating in pulsed mode, and that the mode-locking effect will sustain this pulsed mode. As the resonator of the Kerr-lens mode-locked laser has been optimised, containing a Kerr-lens, it will be less stable for non-mode-locked CW output. Figure 2.5 shows the Kerr-lens principle with a hard aperture, where a large part of the output in CW mode will be absorbed. In the experiment a so called soft aperture is created by the focus of the pump-laser in the TiSa crystal. In the KLM laser the material dispersion of one round trip

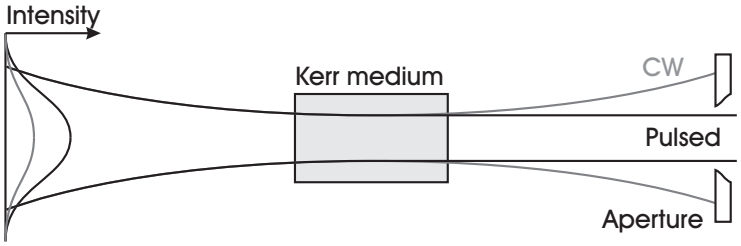

Figure 2.5: hard aperture Kerr-lens mode locking principle

in the laser is compensated by a prism pair placed within the resonator cavity, see figure 2.6. The length of the resonator dominates the repetition rate, in this

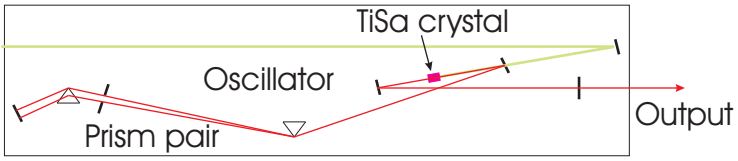

Figure 2.6: Schematic of Kerr lens modelocked laser

case it is set to a repetition frequency of 81.25 MHz. This value is the 16th harmonic of the RF source that drives the linear accelerator at 1.3 GHz, which will be used for synchronisation between the two systems. The pulse duration, after compensation for the last round trip is 25 fs. And typical energy per pulse is 1-3 nJ.

2.2 Stretcher

Amplification of the pulse without stretching it in time will cause damage to the optics, and the amplification of such a short pulse will be less efficient due to self phase modulation and self focussing effects in the amplifier. Stretching of the pulse is performed by an Oeffner stretcher [10][9]. This stretcher design is completely symmetric, so that only symmetrical aberration can appear. The presence of two spherical mirrors whose radius of curvature ratio is two and of opposite sign cancels these aberrations, since all the optics are mirrors. In this optical combination, perfect stigmatism is ensured only when the grating is at

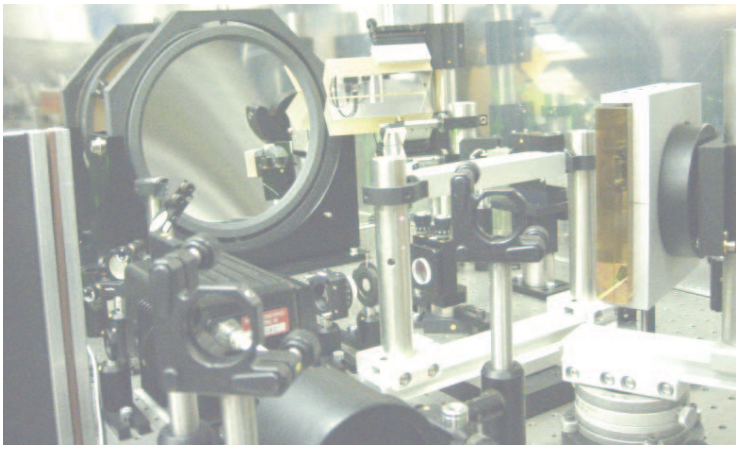

Figure 2.7: Photograph of stretcher

the common centre of curvature. Unfortunately the stretcher will not stretch the pulse when the grating is exactly positioned in this common centre of curvature, but Cheriaux *et al.* [9] have shown that the spherical aberrations introduced by the positioning the grating is away from this centre of curvature is weak enough not to affect the pulse shape. As the design is based on curved mirrors it does not contribute to any material dispersion. The design of the compressor is more intuitive, than that of the stretcher. The only difference between these designs is the additional telescope in the design of the stretcher to create an image of the first grating behind the second grating. According to the definition of an image, all the path lengths to the image are of equal size. This new image of the first grating behind the second grating, creates a "negative" optical distance between the two gratings, and the function of separating the colours in time is inverted compared to the compressor. The figure 2.8 shows how this "negative" optical grating distance (L_g) is created by a simple telescope of two lenses. The

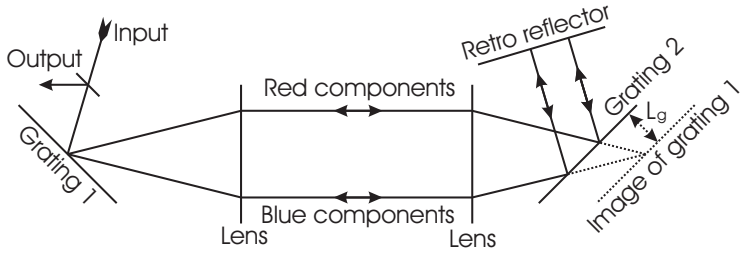

Figure 2.8: Schematic of stretcher

design of the Oeffner stretcher is based on two mirrors, to create the telescope. These mirrors fold the path of the beam, and only one grating is used in this set up. The design has been made by [20] for suitable stretching of the pulse to a suitable length required for the amplification of it. The distance between the first grating and its image, in this design, is 70 cm. The figure 2.9 shows the ray traces through the object, in two dimensions, and originating from earlier simulations in ZEMAX [20]. The ray traces in three dimensions are shown in

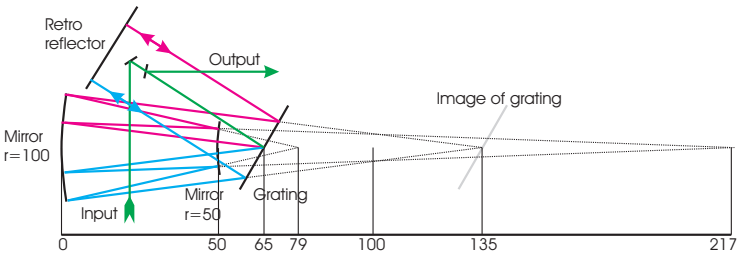

Figure 2.9: Scematic of Oefner stretcher

figure 2.10. A photograph of the stretcher is presented in the beginning of this section in figure 2.7.

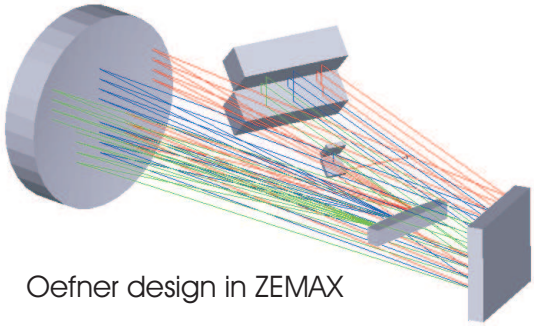

Figure 2.10: Zemax design of stretcher [20]

2.3 Regenerative amplifier

The advantage of a regenerative amplifier is its stable output beam profile which is typically the case for a resonator cavity. Another advantage is the option to let the pulse pass through the crystal many times with a relative low gain per pass, this makes a regenerative amplifier appropriate for pre-amplification of the pulse. The low gain per round trip prevents amplified spontaneous emission (ASE) build-up [3]. Suppression of ASE is required for amplification of a very low energetic pulses to a higher stable energy levels. A Pockels cell is used in the cavity of the regenerative amplifier for in and out coupling of the pulse. Therefore a regenerative amplifier is less suitable for amplification of pulses with a very short pulse duration of 10 fs, due to the dispersion of these materials. Nevertheless, regenerative amplifiers have also been used to generate pulses of 30 fs and shorter duration [8]. Multi pass amplifiers with many passes (8-10) can be used for amplification of pulses with a pulse duration less than 10 fs, as the dispersion introduces by material is much less than of a regenerative amplifier. The disadvantage of the multi pass amplifier is the fact that is does not correct the spatial pulse shape, and the output beam profile is of lower quality. The laser wake field acceleration experiment requires a high quality beam profile for a neat focus of the beam and a pulse duration of 25 fs, this

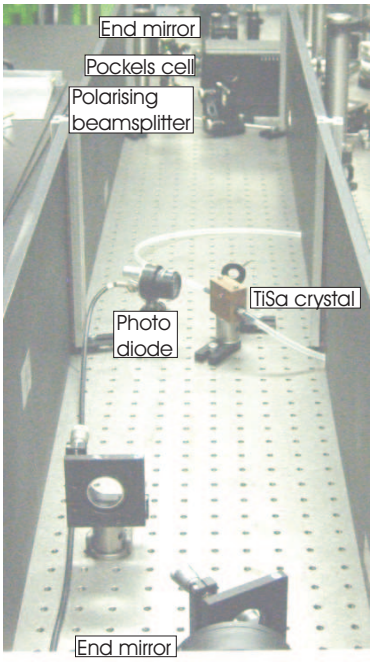

Figure 2.11: Photograph of regenerative amplifier

makes the regenerative amplifier the best choice for pre amplification.

The regenerative amplifier is basically a resonator cavity with an amplification crystal, also TiSa, placed in the cavity. By adjustments to the polarisation direction of the light a pulse from the pulse train can be selected, and coupled into this resonator cavity. After extraction of all the energy from the crystal, the same pulse can be coupled out of the resonator cavity. The in and out coupling of the pulse is done with the combination of a Pockels cell, a $1/4\lambda$-plate and a polarising beam splitter. The latter reflects s-polarised light and transmits p-polarised light. In the meanwhile all the other pulses from the pulse train will not be used. The three schematics in figure 2.12 show the pulse selection process. The only active element used for selection is the Pockels cell, this device is based on birefringence in an optical medium induced by a constant or varying electric field. The Pockels cell used in this set-up can be set to three values, and can act as a non-birefringent material, quarter-wave plate or half-wave plate.
In the first stage the Pockels cell is set to 0 in figure 2.12a. The light is s-polarised and reflected at the polarising beam spliter into the direction of the Pockels cell. The Pockels cell does not change the polarisation, and the $1/4\lambda$-plate is passed two times, changing the polarisation to p-polarisation. The Pockels cell is still switched off, and the p-polarisation of the light will be sustained. The pulse is now transmitted through the polarising beam splitter and propagates towards the crystal.

During the time that the light pulse travels through the left side of the cavity, the Pockels cell is switched to 1 as in figure 2.12b, and acts as a $1/4\lambda$-plate, this in combination with the $1/4\lambda$-plate installed at the right end of the cavity, makes the total half end of the cavity (due to the mirror) act as a full λ plate,

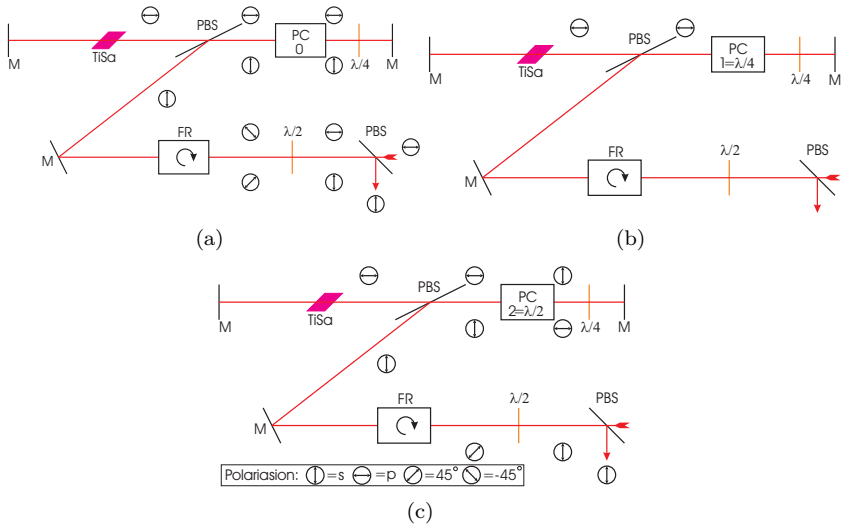

Figure 2.12: Three stages of coupling the pulse in and out of the regen cavity

resulting in no nett polarisation changes. In this manner the pulse is captured in the cavity.
After enough energy has been extracted from the crystal, the pulse can be coupled out of the regen by switching the Pockels cell to 2-mode as in figure 2.12c. Now the Pockels cell acts as a $1/2\lambda$-plate, this in combination of the $1/4\lambda$-plate and the mirror results in a net polarisation rotation of 90° changing the polarisation of the light pulse to s-polarisation. Now the polarising beam splitter reflects the s-polarised light, coupling the amplified pulse out of the regen cavity.
The first half-wave plate used in the set up (not in the regen cavity) is mounted at an angle of 22.5° rotating the polarisation of the incident right from 0° to 45°. In combination with a Faraday rotator this will be further rotated over an angle of 45° to a final angle of 90°. To change the polarisation of the pulse from p (output of the oscillator and stretcher) to s (for incoupling) a Faraday rotator element used in the experimental set up rotates the polarisation of the light over an angle of 45° according to the corkscrew law, therefore the polarisation does not rotate back to its original polarisation when light travels in reverse direction. In this manner the output of the regen cavity can be separated from the input, and will not propagate back into the stretcher. Further information concerning the principle of a Faraday rotator and a wave plate can be found in [12]. More aspects concerning of the regenerative amplifier will be discussed in chapter 3.

2.4 Multi pass amplifier

The design of the laser system includes two multi pass amplifiers. As these multi pass amplifiers are beyond the scope of this master thesis, they are not treated here in any detail. For the complete picture they are briefly discussed here, as the adjustments of the settings are estimated in section 5.5 for the case the

multi pass amplifiers are put into the experimental set-up. These predictions on the adjustment of the compressor show the first advantage of these amplifiers, which is that the dispersion introduced by them is minimal, since the only material dispersion introduced is the TiSa crystal itself. With the help of a set of mirrors the light is redirected several times through the crystal under different angles, see figure 2.13. In this manner the light can pass through the crystal

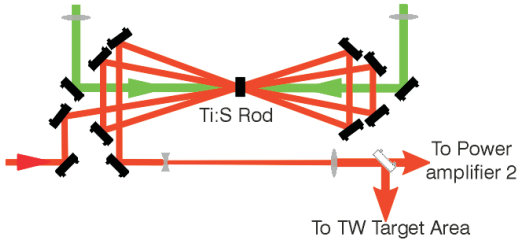

Figure 2.13: Schematic of 4-pass amplifier

several times, and can be coupled out at a different place from where it has been inserted, meaning that no complex polarisation modification is required, and thus the material used for this amplifier is limited to the mirrors and the crystal.

2.5 Grating compressor

A grating compressor is used to re-compress the amplified pulse. To compensate for additional material dispersion, the design of the compressor is based on gratings with a different grating periodicity than the periodicity of the grating used for the stretcher [13]. This is because the analytical equations for the stretcher and compressor are identical except for the sign of the grating distance. The set up of the compressor, shown in figure 2.14, is more intuitive than the design of the stretcher although they are based on the same effects. On the first grating the spectrum of the pulse is diffracted over a cone. The second grating, positioned at the same angle as the first, let all the spectral components travel parallel to each other. The retro reflector redirects the light back to the second grating, inverting the process. Due to the effect that the different spectral components have travelled over different distances, the stretched pulse can be re-compressed. More details and measurements of the compressor are presented in section 4.2.1.

2.6 Grenouille

For measurements on the shape of the ultra short output pulse, no direct detectors are available. Therefore instruments like a Grenouille can be used to generate a representation of the pulse, whereof the shape in time of the pulse can be derived. This instrument is used to optimise the compressor settings in the experiment to minimise the dispersion of the set up. This section will first briefly discuss the principle of an auto correlator and a Frog, in order to create

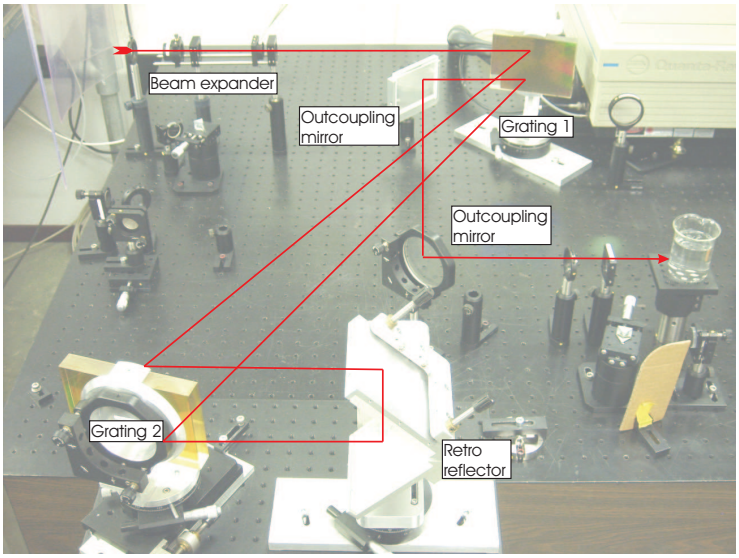

Figure 2.14: Photograph of compressor

a better explanation of the Grenouille instrument. More detailed information on measurement techniques for ultra short light pulses can be found in [14].

The most simple measurement technique for measurements on ultra short pulses is an auto correlator. This device splits the power of the laser pulse into two equal parts, whereof one part travels a different path length. The detector used is based on non-linear response. In most simple cases a LED is used, as 2-photon absorption processes in the diode generate an electric signal. Tuning of the path length difference of the two pulses the overlap of the two pulses can be tuned. The detector output signal will be a function of this overlap. Figure 2.15 shows a basic design of an auto correlator, this type of auto correlator requires a train of pulses to acquire the whole pulse structure. To reveal the spectral

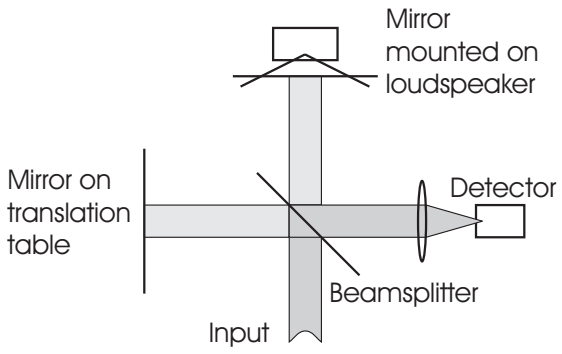

Figure 2.15: Scematic of autocorrelator

information from an ultra short pulse, it is possible to replace the detector by a

thin SHG crystal, also a non-linear response, in this crystal frequency-doubled light is generated. Analysis of the spectrum of the generated light by a prism or grating will reveal the moment of arrival of the spectral components. A device of this type is called Frequency Resolved Optical Gating, FROG, shown in figure 2.16. For easy measurements on single shots, another apparatus can

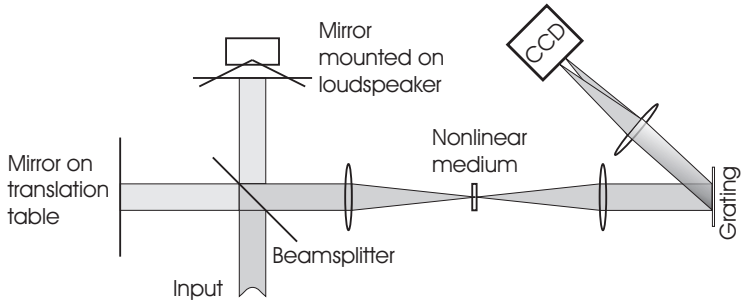

Figure 2.16: Schematic of Frog set up

be used, the Grenouille[1]. The advantage a Grenouille is its simple construction, and it is easy to align. Three parts of the frog have to be replaced; the auto correlator, the thin SHG crystal and the spectrometer. This means that none of the components of the FROG remain. The auto correlator has to be replaced by a Fresnel bi-prism. When a beam of a large diameter travels through a Fresnel bi-prism, it will be split into two bundles crossing each other, shown in figure 2.17. In this manner the time delay between the two pulses is projected in the horizontal direction.

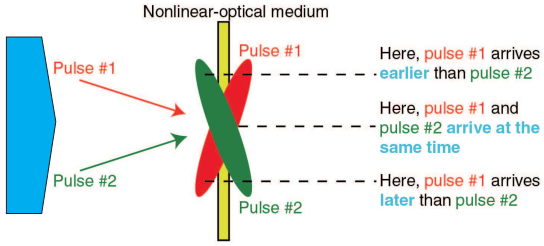

Figure 2.17: Pulse through the bi-prism, generating the time scale in the horizontal direction

The thin crystal and the spectrometer are replaced by a thick crystal and a cylindrical lens in the vertical direction. Now for generation of higher harmonic light one has to obey the phase matching condition within the crystal. This can be performed by tuning of the crystal angle. This tuning of the angle of the incident light on the crystal is performed by the cylindrical lens, and therefore the crystal will act as a spectrometer spreading the spectrum in the vertical direction. Only two extra cylindrical lenses are used to project both the spectral as the time resolved information of a single pulse on a CCD-camera, see figure 2.18. Measurements on the pulses are presented in the two dimensional image,

[1]GRENOULLE is the acronym for: Grating-Eliminated No-nonsense Observation of Ultrafast Incident Laser Light E-fields. GRENOUILLE, which is the French word for "frog".

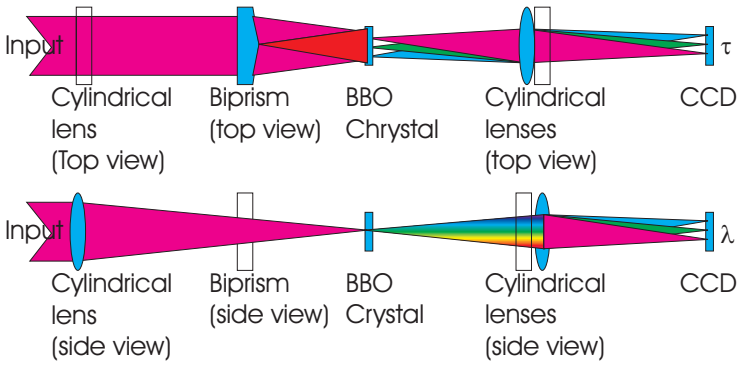

Figure 2.18: Pulse through Grenouille observed from the side and from the top

and analysed by a computer program[2]. This program analyses the image, and after calibration of the program, it returns a value for the pulse duration and spectral width of the pulse. Beside these generated numbers, the image itself provides a good sense for the pulse shape. Measurements on the output of the pulse have been performed, and the calibration and the measured results are presented in section 6.

[2]The program used, called "Video Frog", has been obtained from Mesa Photonics, LLC, Santa Fe, USA. www.mesaphotonics.com.

CHAPTER 3

Pulse amplification in detail

An advantage of chirped pulse amplification is the possibility of amplification of ultra short pulses to very high energies. The amplifier will saturate at higher energy levels and damage to the optics can be avoided due to the stretching of the pulse. Some disadvantages are also introduced by this method, besides narrowing of the spectrum due to the gain, also walk off of the central frequency occurs. Driving the amplifier to a saturated level can compensate for some of these disadvantages, as this broadens the bandwidth of the amplifier. It also becomes less sensitive for the input energy, suppressing the fluctuation of the output energy. This chapter will treat these effects by simulations, and analyses to what degree this occurs in the experiment.

3.1 Bandwidth of the regenerative amplifier

It is of vital importance to maintain the bandwidth of the pulse, since the spectral bandwidth is a measure for the Fourier transform limited pulse duration. The bandwidth of the regenerative amplifier is limited by the bandwidth of the crystal. In this case a titanium-doped sapphire (TiSa) crystal is used to amplify the seed pulse from the oscillator. Since the oscillator is also based on a TiSa crystal the bandwidth matches well. But even then, due to the effect that the wings of the spectrum are less amplified than the centre, the bandwidth of the output pulse narrows during amplification. For example see figure 3.1 [3].
This gain narrowing effect is well visible in simulations performed with Lab2[1]. This simulation is an optical tool kit that runs within the Labview environment. The sub-vi's (routines) of the Lab2 tool kit are all designed to perform simulations on ultra short laser pulse systems. The routines of the Lab2 package offer elements which are designed for simulation of short pulse laser systems. Therefore the Lab2 package is used to model the gain narrowing of the experimental set-up. In this model a short laser pulse is amplified by a regenerative amplifier, which is also the case in the experiment. For simplicity reasons the stretcher is not included in this simulation, as this device had no influence on the results of

[1] It is possible to download this free-ware simulation package from *www.lab2.de*

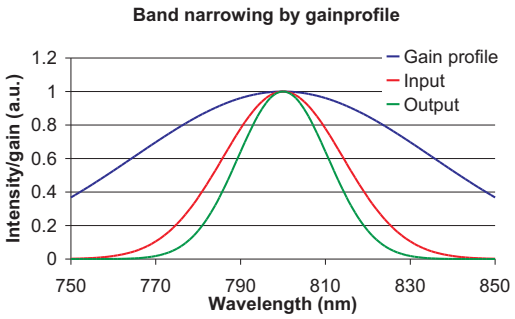

Figure 3.1: Gain narrowing

the simulation. The schematic of the simulation made in Lab2 is as shown in the picture 3.2. The program is also put in the appended CD, appendix B.

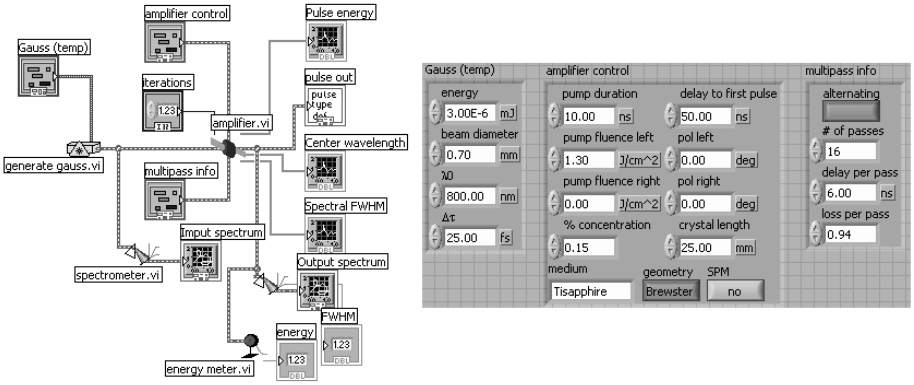

Figure 3.2: Schematic of regenerative amplifier in Lab2, with used input parameters

This program simulates the evolution of the pulse properties during the amplification in the regenerative amplifier. As input pulse a representive pulse for our set-up of 25 fs has been put into the regenerative amplifier, the input parameters are shown in the screen shot in figure 3.2. In this simulation we are mainly interested in the spectral development of the laser pulse during amplification Dispersion and pulse duration are not of interest in this simulation. Three measurable values can be used for comparison of this simulation with the experiment; the built up of energy in the regen, the output energy and the shape of the spectrum. The energy of the pulse, built up in the regenerative amplifier can be monitored in the experiment by measuring the reflected light at the Brewster windows of the crystal with a photo diode. Also the output energy and spectrum of the regenerative amplifier can be measured and compared to the simulation output. Analysis of the simulated pulse energy build up in the regenerative amplifier and the simulated output energy agree well with these monitors in the experiment. Figure 3.3 show the development of the pulse energy as function of the number of round trips through the regen

cavity, as well in the experiment as in the simulations. Note that after one period in the measurements the pulse has travelled two times through the crystal ($N_{roundtrips} = 2 \cdot N_{pass}$).

The output power of the regenerative amplifier can be increased by shifting the

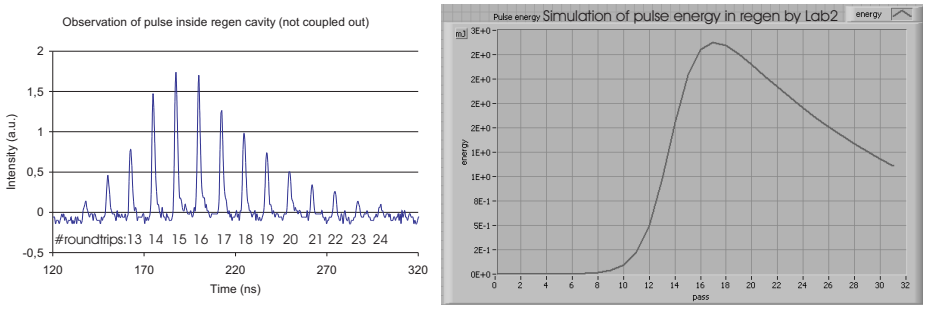

Figure 3.3: Pulse energy during amplification, simulated and measured

focus of the pump beam in the direction of the crystal, but the output power should not exceed the value of 5 mJ, as damage to the Faraday rotators occurred at energy levels of 7 mJ. The simulation shows a lower value of the output energy, than measured values of the experiment. The reason for this difference is not known. Perhaps this could be due to the fact that the simulations are not performed on a chirped pulse, which lowers the fluency, and that saturation of the crystal occurs at a higher pulse energy level in the experimental set-up. This may explain the difference in round trips, as the pulse passes the crystal approximately two times more in the experiment.

Comparison of the simulations of the spectral development show disagreements with the measured output, as these showed walk off of the central frequency. But the simulation also shows some other remarkable effects like narrowing and broadening of the spectrum during amplification, as observed in figure 3.4. The main reason why there are some disagreements, is that the simulations are not based on a chirped pulse amplification. Amplification of chirped pulses show a strong walk-off of the central wavelength, due to the fact that in our case the red components precede the green components and deplete the gain. Therefore the green components are less amplified resulting in a strong spectral shift to the red. As Lab2 is mainly designed to simulate the dispersion of the set-up, it is based on effects in the spectral domain. The spectral shift that occurs during chirped pulse amplification, is an effect in the time domain. Unfortunately this effect of frequency shift is not included in the Lab2 package.

Lab2 has an option to calculate another effect in the time domain; self phase modulation (SPM). Self phase modulation occurs due to change of refractive index caused by high peak intensities, introducing spectral phase disturbances to the output pulse. In our set-up this is not the case as its peak intensity is lowered by stretching the pulse. Reducing the SPM by stretching the pulse is not simulated in Lab2, therefore this function has been switched off. To discuss the spectral development of the pulse during amplification one has to keep these boundaries of Lab2 in mind.

The development of the spectral width shows a remarkable effect. In the first round trips gain-narrowing occurs, but in the latter passes a spectral broadening

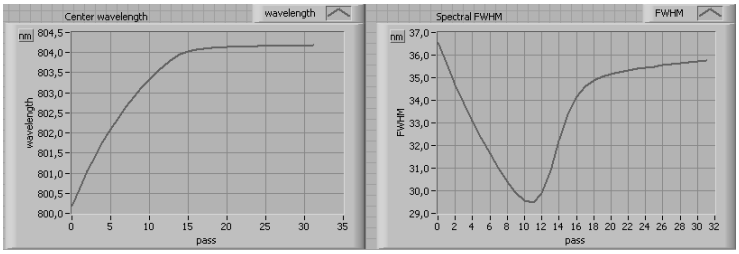

Figure 3.4: Spectral development simulated by Lab2

effect takes place, see figure 3.4. The high intensity of the centre wavelengths saturate the crystal, and will not be amplified to the full extent. The wings of the spectrum have not reached this saturation value yet, and therefore the spectrum broadens during these last passes through the crystal until all the energy has been extracted from the crystal. Excessive pumping of the crystal drives this effect to a further extent, and simulation with a pump fluency of 2 J/cm^2 show a faster saturation process, and due to the extra energy in the crystal the amplification of the side bands proceeds to a further extent resulting in an output pulse with a broader spectrum than the input pulse. This effects is called homogeneous broadening, is caused by the saturation of the amplifier as discussed in [15].
These results show that it is important to saturate the amplifier as far as possible, and extract the pulse just before the output power starts to reduce. In this manner the spectral output width has a maximum value which is important for generation of a Fourier transform limited pulse length. In the experiment the pulse is extracted just after the highest pulse energy, so that the fluctuation of pulse energy is much smaller.

Lab2 does not accurately simulate the amplification of a chirped pulse. In the experiment the central frequency walks off into the red direction, running it into the boundary of the gain profile. Adding the effects of gain narrowing and shifting due to chirped pulse amplification results in a shifted and narrowed spectrum of the output pulse, as shown in measurements 3.5a. Figure 3.5b shows the output of the pulse after recompression; here the bandwidth seems to be shifted more to the centre again, which might be due to the fact that the compressor does not support the complete spectrum.

It is possible to reduce the spectral gain shifting and narrowing, by placing an etalon in the regenerative cavity. In this manner a band filter is created, forcing the spectrum to the demanded value. Although this experiment is not part of this thesis, the first results are presented in figure 3.5c. This figure shows that the main lobe did shift into the blue direction, satisfying the theory of manipulating the spectrum. The figure shows that the spectrum can be divided into different lobes. It is recommended to add a second etalon tuned at a different angle to suppress this second lobe. Perhaps it is also possible to create a dip in the centre of the spectrum, to broaden the spectrum.

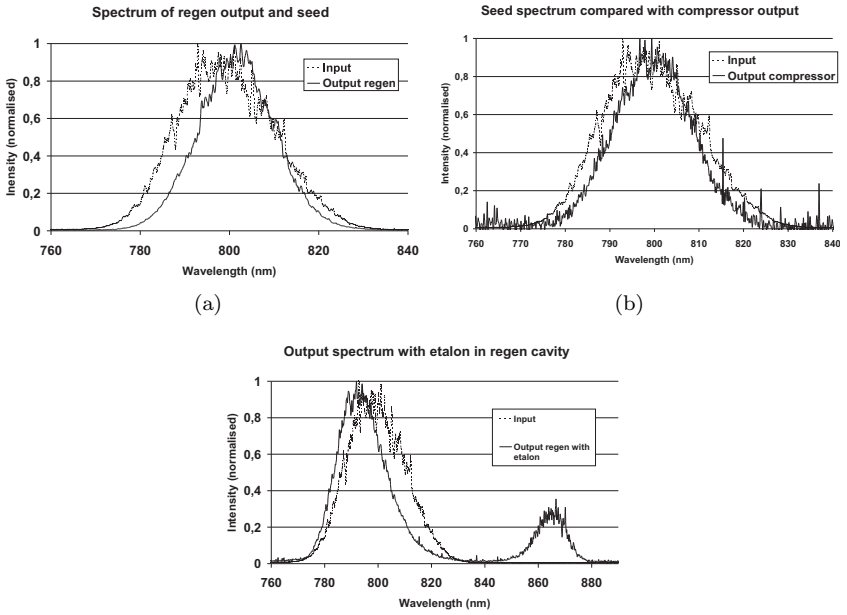

(a) (b)

(c)

Figure 3.5: Spectrum of the amplified pulse compared to the spectrum of the input pulse in three situations; after the regen, after re-compression and with an etalon in the cavity.

3.2 Analysis of beam propagation

For the design of the optics after the regenerative amplifier the properties of the beam in the regenerative amplifier have to be well defined. One way of determining the beam parameters is to calculate the properties of the resonator. From the resonator parameters the beam parameters can be deduced. The easiest way is to solve the geometrical properties of the resonator. A slightly more advanced method is to calculate the q-parameter of the resonator by the (ABCD)-matrix of the resonator, the advantage being that this method can be adjusted by adding simple elements to the system. To be really sure what the beam properties in the experiment are, the beam has been observed with a camera in order to determine the beam properties.

3.2.1 Calculation of the beam properties by the resonator properties

The parameters for a Gaussian beam are the length of the beam waist z_0, the size of the waist w and the curvature of the wave front R. The radial intensity profile of a Gaussian beam is described with:

$$I(x,y) \cong e^{-2\cdot\frac{x^2+y^2}{w^2}} = e^{-2\cdot\frac{r^2}{w^2}}, \tag{3.1}$$

where $r = \sqrt{x^2+y^2}$. Most programs measure the full width half maximum (FWHM) of the Gaussian beam profile, the conversion between FWHM and

waist is:

$$w = \frac{FWHM}{\sqrt{2 \cdot ln(2)}} \approx \frac{FWHM}{1.1774} \tag{3.2}$$

In the first approach to calculate the beam properties of a stable resonator equations are used from [17], where the authors utilise the fact that in a resonator the curvature of the wave front is equal to the curvature of the mirrors. With these statements the beam properties of a stable resonator as function of the resonator geometry can be generated. The minimum waist w_0 of the beam is given by

$$w_0 = \frac{(\frac{\lambda}{\pi})^{1/2}[L(R_1 - L)(R_2 - L)(R_1 + R_2 - L)]^{1/4}}{(R_1 + R_2 - 2L)^{1/2}}, \tag{3.3}$$

with, L the resonator length, λ the wavelength of the used light, R_1 and R_2 the curvature of the resonator mirrors. Once the w_0 and the wavelength of the light is known, the waist $w(z)$ at position z along the optical axis can be derived with:

$$w(z) = w_0\sqrt{1 + z^2/z_0^2}, z_0 = \frac{\pi w_0^2}{\lambda} \tag{3.4}$$

Here the Rayleigh length, is z_0. The divergence angle θ can be derived with:

$$\theta = \frac{\lambda}{\pi w_0} \tag{3.5}$$

All these parameters describe the path of a Gaussian beam. Figure 3.6 presents a small overview of all these parameters.

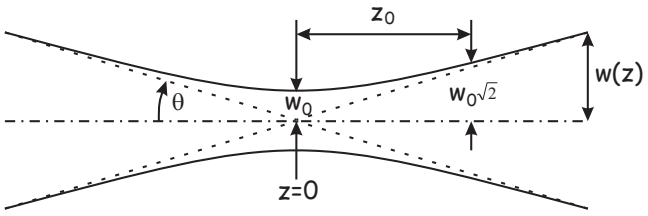

Figure 3.6: Properties of a beam.

3.2.2 Calculation of the beam properties with use of the (ABCD)-Matrix

Another way of calculating the beam properties is by determining the q-parameter directly out of the optical system matrix. The q-parameter describes the propagation of the beam. The q-parameter is defined by:

$$\frac{1}{q(z)} = \frac{1}{R(z)} + \frac{i\lambda}{\pi w^2(z)} \tag{3.6}$$

The following equation is applied to determine the output q_f of an optical system ((ABCD)-matrix) and its input parameters q_i:

$$q_f = \frac{Aq_i + B}{Cq_i + D} \tag{3.7}$$

One special case of this is a resonator mode. For example, if one takes the q-parameter of a stable resonator mode in the resonator cavity, one can imagine that the q-parameter after one full cycle through the cavity is exactly identical to the initial q-parameter. Otherwise it would not have been a stable mode. This case is sketched in figure 3.7. Here one can see that the curvature of the

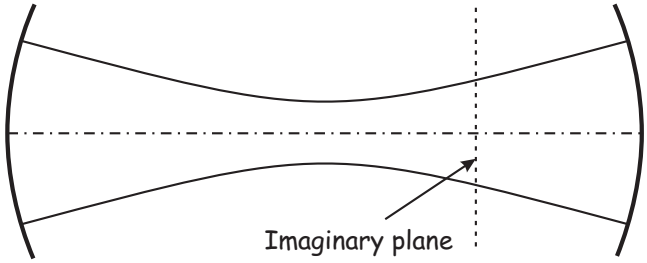

Figure 3.7: Laser resonator, with stable mode.

wave front is equal to the curvature of the resonator mirrors. The q-parameter at an imaginary plane chosen at an arbitrary position on the optical axes is exactly the same after one complete cycle through the resonator. This reduces equation 3.7 to a more simplistic one:

$$q(z) = \frac{Aq(z) + B}{Cq(z) + D} \tag{3.8}$$

In this form the q-parameter can be extracted as function of the elements of the ABCD-matrix (ie. resonator configuration). Separating the imaginary part from the real part of this solution and coupling these solutions to the definition of the q-parameter 3.6, the beam parameters can be determined. One advantage of this method is the fact that one can easily change the resonator configuration, by addition of extra elements in the resonator. The only part that has to be adjusted is the (ABCD)-matrix of the system.

3.2.3 Measurements on the waist

In order to compare the theoretical value of the beam waist with the experimental value one has to measure the beam waist. To perform an accurate measurement, the development of the beam waist in the propagation direction has to be determined. This has been done by measuring the beam waist at several points along the optical axis. This data can then be fitted to the theoretical model for the development of a Gaussian beam eq. 3.4. From this fit the waist w_0 and its position z can then be obtained with a high accuracy. In order to perform a well defined measurement of the regenerative amplifier, it is preferable not to let it operate in free oscillating mode, but instead with an inserted seed. This can be done by placing two beam samplers at an angle of ninety degrees in the beam path, from which the output of the regen can be seen in the reflection, while the seed can still be inserted in the regen, as shown in figure 3.8. The camera is read out by a routine that determines the full width half maximum (FWHM) of the beam in the horizontal and the vertical direction, and logs these values in a file.

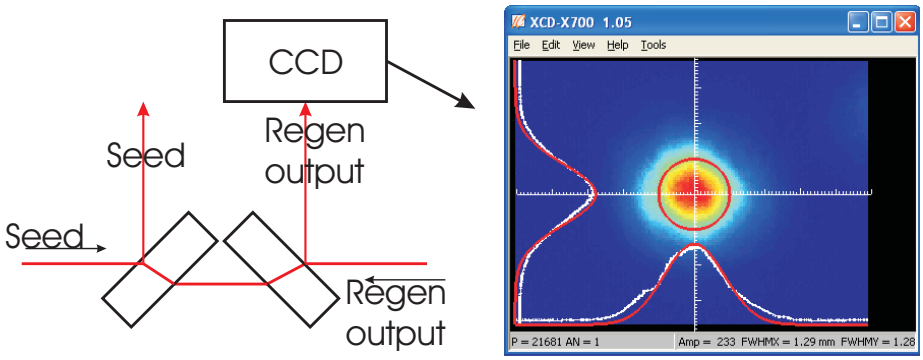

Figure 3.8: Measurement on output beam, with typical beamprofile

3.2.4 Results of measurements on waist compared to theoretical values

Every point along the beam path has been measured over approximately one minute with a repetition rate of 10 Hz, and the final results per point along the beam path is based on the average of these measurements. The accuracy of the measurements has been defined by the standard deviation of these measurements and are presented in the error-bars of figure 3.9. The error in the positions of the

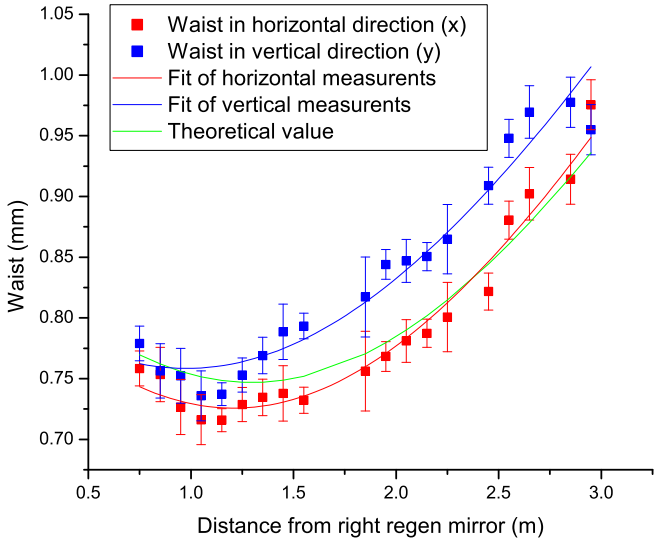

Figure 3.9: Measured results

measurements is less then one centimetre. The reference point of the positions (z) of the measurements is the first regen cavity mirror. The position of the first measured point made at 0.5 meters, as this is the closest point after the polarising beam splitter where the pulses exit the regen. The measured points

are performed over a distance of 2 meters up to the position of 2.5 meters from the first regen cavity mirror, see figure 3.10. The measurements showed an

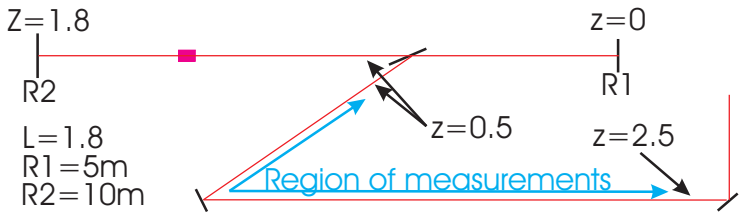

Figure 3.10: Region where the beamwaist has been measured

oval beam profile, so that the measured results are presented in both horizontal and vertical direction direction. Figure 3.9 shows the measured values of the beam waist (dots) and their fit to the theoretical model presented in equation 3.4. The derived values for the corresponding beam parameters are presented in table 3.1. The green line originates from the model for a similar resonator cavity as described in section 3.2.1. This comparison of the fitted measurement

Measured of waist size and its position		
Direction	waist w_0 (mm)	Position z (m)
horizontal	$0.73 \pm 5 \cdot 10^{-3}$	1.2 ± 0.04
vertical	$0.76 \pm 6 \cdot 10^{-3}$	0.98 ± 0.04

Table 3.1: Fitted beam parameters to the measurements

with the theoretical beam parameters reveals a slight difference in position of the beam width. This difference of the position of the beam waist could be caused by several errors in the simple model for the resonator of the regenerative amplifier. One reason could be the thermal lensing effect of the crystal. Since this crystal is pumped with a high energy pulse and water-cooled on the outside, the temperature distribution is not homogeneous over the crystal surface. This can induce an extra thermal lens effect of the crystal. To analyse this, the model based on matrix calculation is used, the calculations can be found at the appended CD, appendix B. Here a new matrix is made of the resonator, but now including a weak lens at the position of the crystal. After adjusting the focal length of the lens, the simulated position of the beam waist became more in accordance with the measured one. Again this simulation has been performed for horizontal direction and vertical direction. The table 3.2 presents the comparison between the measured values and the model discussed in section 3.2.2. But these results do not cover the differences in beam waist and other effects taking place. The TiSa crystal is placed at the Brewster angle, and it is known that Brewster windows cause astigmatism [11]. This effect could explain these disagreements of the measured beam properties with the theoretical ones. But this has not been explored in more detail. Fortunately the asymmetry of the beam profile is very small, and almost not measurable, therefore it would not affect the outcome of the experiment.

Comparison of measurements with the model including thermal lensing					
Direction	Focal length	Property	Theoretical value	Measured value	Difference
Horiz.	f=40 (m)	w_0 (mm)	0.74	0.73	0.01
		z_0 (m)	1.21	1.21	0.0
Vert.	f=9.75 (m)	w_0 (mm)	0.71	0.76	0.05
		z_0 (m)	0.98	0.98	0.0

Table 3.2: Comparison of measured beamwaist and its position with the values generated by the (ABCD)-matrix model that includes thermal lensing.

CHAPTER 4

Compensation of dispersion

Dispersion is the dissociation of light, and has a destructive effect on short light pulses, therefore it plays an important role in amplification of ultra short light pulses.

4.1 Introduction

Opera singers are very good at singing one single tone for a long time. It is rather easy for the listener to determine the frequency of this tone. But determination of the acoustical frequency of one clap in the hands, is more difficult. This is due to the fact that the clap is a short event in time, and therefore consists of a wide range of frequencies. Fourier observed this aspect a long time ago and developed a transformation routine to transform events in time into its frequency components. He based this transformation on the observation that all the signals could be decomposed into a weighted sum of much simpler single frequency components (sinusoidal signals). This relation shows that short events, in this case in time, contain many different frequency components. The Fourier transformation of signals in time, t, to their spectral components, ω, can be performed with:

$$F(\omega) = \frac{1}{2\pi} \int_{-\infty}^{\infty} f(t) e^{-j\omega t} dt, \tag{4.1}$$

The inverse Fourier transformation performs the exact reverse action and recreates the signal in time out of the spectral information:

$$f(t) = \int_{-\infty}^{\infty} F(\omega) e^{j\omega t} d\omega \tag{4.2}$$

In physics many signals are approximated by a Gaussian shape. One of the reasons to model these signals with this Gaussian profile is that a Fourier transform of a Gaussian signal has a Gaussian shape as well. The following Gaussian signal with pulse duration τ_p;

$$f(t) = e^{-\frac{t^2}{2\tau_p^2}}, \tag{4.3}$$

can be Fourier transformed according equation (4.1) to:

$$F(\omega) = \frac{\tau_p}{\sqrt{2\pi}} e^{-\frac{\omega^2 \tau_p^2}{2}} \tag{4.4}$$

Which is also a Gaussian profile, but its spectral width scales with the inverse of the time duration τ_p, as expected. The relation between the spectral FWHM[1] ($\triangle\omega$) and the FWHM of the time duration ($\triangle t$) can easily be calculated as follows:

$$e^{-\frac{(\frac{1}{2}\triangle t)^2}{\tau_p^2}} = \frac{1}{2} \Rightarrow \triangle t = 2\tau_p\sqrt{ln2} \tag{4.5}$$

$$e^{-(\frac{1}{2}\triangle\omega)^2\tau_p^2} = \frac{1}{2} \Rightarrow \triangle\omega = 2\frac{\sqrt{ln2}}{\tau_p} \tag{4.6}$$

Multiplication of these half widths gives the relation between the spectral width and the time duration of Gaussian shaped signals.

$$\triangle\omega \cdot \triangle t = 4ln2 \tag{4.7}$$

This relation alone is not enough to describe a short pulse, although a tungsten light bulb has a very broad bandwidth, it does not produce short pulses. In order to produce short pulses the different colours from the light must arrive at the same time and place. Since we are speaking about waves in this case it is more easy to state that all the different waves, having different wavelengths, should all have one of their maxima coincide with each other to have full positive interference at that particular time and place. This is also visualised in figure 4.1. As this positive interference occurs at the scale of wavelengths this is also called the spectral phase relation of the light waves. As lamb bulbs emit no coherent light, creation of this phase relation is impossible. Lasers on the contrary can produce coherent light. The disadvantage of a simple laser is its narrow the spectral bandwidth. Mode locked lasers have been developed to overcome these problems. They combine a broad spectral width with the coherency of laser light. In this manner these lasers can produce ultra short laser pulses with a well defined spectral phase relation. Figure 4.1 shows the difference between random added colours, and a sum of colours with a phase relation. Once an ultra short pulse has been created, it is of vital importance to conserve the spectral phase relation. The pulse length will be affected by disturbances in the spectral phase. When light travels through a dispersive medium like glass the red spectral component will travel faster than the blue spectral components, in this manner the pulse will be stretched, as the spectral components arrive at different times at the detector, as shown in figure 4.2. This separation of spectral components in time is called chirp[2]. Linear spectral phase disturbance does not affect the pulse shape, it only introduces a delay in travel time through the medium. The following images show sinusoids with different frequencies and the sum of these sinusoids compose a pulse in time as in figure 4.3. In the second image a linear spectral phase has been introduced and the sum of signals show that the pulse energy has been shifted to the side, which means that an extra time delay has been generated. Unfortunately most

[1] Full Width Half Maximum

[2] The name "chirp" origins from the sound of a bird, as most birds sing a scale of tones in one call. Starting with low tones and scaling up to higher ones.

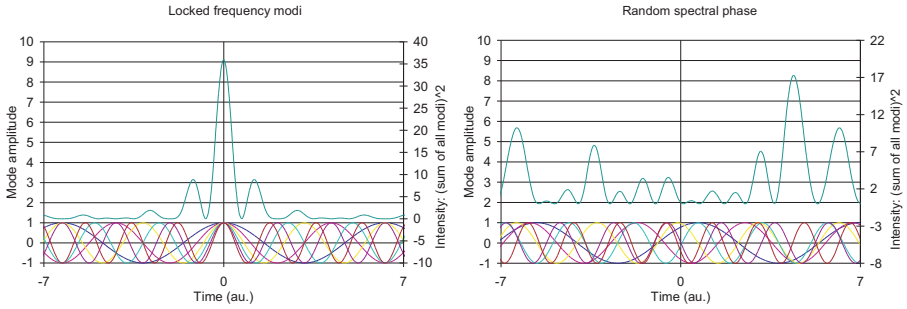

Figure 4.1: Sum of locked and random spectral phases

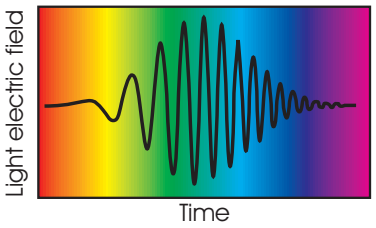

Figure 4.2: Impression of chirped pulse

materials introduce a rather complex spectral phase disturbance ($\phi_{mat}(\lambda)$), due to their wavelength (λ) dependent refracted index ($n(\lambda)$). This spectral phase disturbance scales linear with the length of the material (l_{mat}).

$$\phi_{mat}(\lambda) = \frac{2\pi n(\lambda) l_{mat}}{\lambda} \tag{4.8}$$

Since the linear spectral phase disturbance has no influence on the pulse duration it is interesting to determine the types of spectral phase disturbances that do destructively affect the pulse shape. Therefore it is convenient to start with an input pulse in the time domain, and analyse the deformation of the pulse after it has passed through a dispersive system, as described in [3]. An arbitrary input pulse in the time domain can be written as:

$$E(t) = \xi(t) e^{i[\omega_0 t + \sigma(t)]}. \tag{4.9}$$

Here the slowly varying envelope is $\xi(t)$ and the central carrier frequency is ω_0, while the $\sigma(t)$ is the temporal phase. In case of a Gaussian pulse where $\xi(t) = \xi_0 e^{-(t^2/\tau^2)}$ and $\sigma(t) = 0$, the expression for the input pulse changes to:

$$E(t) = \xi_0 e^{-(t^2/\tau^2)} e^{i\omega_0 t} \tag{4.10}$$

The Fourier transform of this Gaussian pulse gives us the corresponding amplitude and phase in frequency space,

$$G(\omega) = \int_{-\infty}^{\infty} E(t) e^{-i\omega t} dt = g(\omega) e^{i\eta(\omega)} \tag{4.11}$$

Where $g(\omega)$ and $\eta(\omega)$ are the spectral amplitude and phase, respectively. This is a more convenient form for the discussion of the spectral phase disturbances

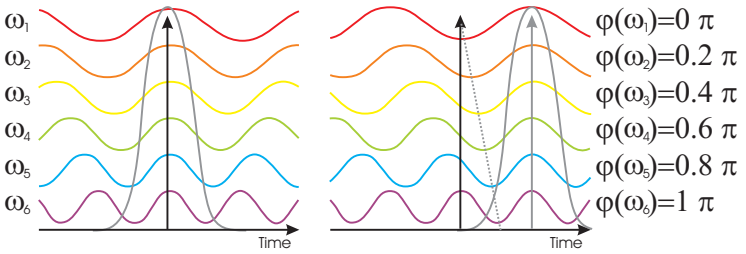

Figure 4.3: Visuatisation of pulse delay due to linear spectral shift

introduced by materials. The output in the spectral domain of the system is then simply:

$$G'(\omega) = G(\omega)S(\omega) = g(\omega)s(\omega)e^{i[\eta(\omega)+\phi(\omega)]}. \tag{4.12}$$

Here the complex transfer function $S(\omega)$ includes the spectral transfer function ($s(\omega)$) and the spectral phase contribution ($\phi(\omega)$) of the system. At this point the spectral phase contribution ($\phi(\omega)$) is of main interest, since this term has a large influence on the pulse shape at the output of the system in the time domain. The spectral transfer function ($s(\omega)$), describes the spectral amplification or attenuation of the system. The $s(\omega)$ term does not affect the spectral phase relation. For this reason this term has not taken into account during the design of a dispersion free system. It does affect the bandwidth of the system, as discussed in section 3.1. The pulse shape in the time domain $E'(t)$ after passing through the system can then be derived by applying inverse Fourier transform:

$$E'(t) = \frac{1}{2\pi}\int_{-\infty}^{\infty} G'(\omega)e^{i\omega t}d\omega \tag{4.13}$$

Note that when a dispersive free system has been created, the output pulse has the same shape as the input pulse.
Now the main target is to determine the $\phi(\omega)$ of the optical system. This spectral phase disturbance depends on the refracted indices of the materials used. Those material properties are all functions of the wavelength, and are rather complex. Taylor expansion can be applied to the spectral phase. This affects the accuracy of the calculations, but minimises the complexity to an acceptable level. Attempts to avoid this simplification step resulted in expressions, that were too complex to solve manually or with the help of programs like Maple. Fortunately the accuracy of the Taylor approximation is sufficient to optimise the set-up for a minimum of dispersion. The following expression shows the Taylor series of the spectral phase:

$$\phi(\omega) = \phi(\omega_0)+\phi'(\omega_0)(\omega-\omega_0)+\frac{1}{2}\phi''(\omega_0)(\omega-\omega_0)^2+\frac{1}{6}\phi'''(\omega_0)(\omega-\omega_0)^3+... \tag{4.14}$$

The main interest here is to analyse the deformation of the light pulse in the time domain. The main disturbance here is that some spectral components travel faster through a medium and stretch the pulse length. Therefore we are mainly interested in the transit time of the spectral components through a medium. The change of the phase introduced by material is given by

$$\phi(\omega) = \frac{L_{mat}n(\omega)}{c}\cdot\omega, \tag{4.15}$$

where the travel time through the medium is $T(\omega) = \frac{L_{mat} n(\omega)}{c}$. Then the transit time through a dispersive medium becomes:

$$T(\omega) = \frac{\delta\phi(\omega)}{\delta\omega} \tag{4.16}$$

The transit time of a quasi monochromatic wave is then:

$$T(\omega) = \frac{\delta\phi(\omega)}{\delta\omega} = \phi'(\omega_0) + \phi''(\omega_0)(\omega - \omega_0) + \frac{1}{2}\phi'''(\omega_0)(\omega - \omega_0)^2 + ... \tag{4.17}$$

Here the derivatives of the spectral phase with respect to frequency: ϕ', ϕ'' and ϕ''' are respectively known as the group delay dispersion (GDD), group velocity dispersion (GVD), third order dispersion (TOD), etc. Just like the figure 4.3 predicts, the linear element of the spectral phase (GDD) only introduces a delay in transit time, but the higher order components introduce independent transit times for the different spectral components around the central frequency, and smear out the power of the pulse in the time domain. An impression of a chirped pulse due to GVD shown in figure 4.2 [3]. When a Gaussian shaped pulse contains no GVD and higher order dispersion, the pulse is called Fourier transform limited, as the inverse Fourier transform of this Gaussian pulse produces the same pulse shape as the input pulse.

4.2 Dispersion compensation

In order to create high power ultra short pulses it is of vital importance that the system does not introduce second- and higher order dispersion as shown in the previous paragraph. The used pulse amplification system, called chirped pulse amplification (CPA), is based however on introducing chirp in a controlled manner. Therefore modelling of the dispersion is an important issue. Modelling of the set-up was mainly performed in programmes like the Disperse-O-Magic (DOM) [18] and by a numerical model in Mathcad [20]. During the construction period of the regenerative amplifier, the design was altered and a review of the model had to be performed. The laser system consists of a stretcher, amplifier and compressor. Because different gratings are used in the designs of the stretcher and the compressor they don‘t fully compensate for each other. In this manner higher order dispersion, introduced by the materials used in the set up, can be compensated [13]. The easiest way for fine tuning the dispersion of the system to a minimum, can be performed by changing the parameters of the compressor. The mathematical models used showed some ambiguous results. DOM for example shows an optimisation number, but this number is only based on the GVD. This means that it is possible to compensate a false property by another, creating more than one unique solution. With Mathcad the circulation of many versions caused some misunderstandings, apparently minor differences in the program creates large differences in the result. Two of these solutions have been built without satisfactory results. Another program based on an analytical model of the dispersion behaviour of the system has been written in Maple. This to fully comprehend the physics and to find an unambiguous solution to this problem.
The philosophy behind the choice of using Maple to create a new model, is the fact that all the current models are based on numerical calculations. Maple

performs the calculations in an analytical manner, this is only possible when the models of the dispersive element are also represented in an analytical manner. For this reason a analytical model is used to describe the spectral phase of the stretcher and compressor. The Sellmeier equations can also be differentiated in an analytical manner. This analytical approach makes it possible to plot several parameters with arbitrary chosen input parameter, without recalculation of the whole model. This option makes it easy to plot a dispersion landscape for the dispersion terms as function of the settings of the compressor like its grating angle and grating separation distance. The visualisation of the dispersion would create much more feeling for the behaviour of the experimental set-up.
In order to design the compressor to compensate the system dispersion three steps have to be taken into account to produce a model and to calculate the optimal settings of the system.

- Inventory of the dispersive elements in the set up
- Putting the gathered data in one mathematical model
- Find the optimal settings

4.2.1 Inventory of the dispersive elements in the set up

To make an inventory of the dispersive materials, all of the material lengths as well as its type had to be determined. Many materials were well defined, some had to be measured and in a single case it had to be estimated. Table 4.1 presents the material lengths in centimetres of our set-up. The names used

Length in cm of dispersive materials used in the experimental set-up					
Element	o-DKDP	BK7	TGG	e-Calcite	o-TiSa
In the oscillator					
TiSa crystal (TS1)					0.5
Cavity mirror (M6)		0.95			
Outside the regen					
Beam splitter (PBS1)		0.7728			
Faraday rotator 2x (FR2)			4		
Faraday isolator (FR1)			2	3.332	
Beam sampler (BS3)		0.566			
Beam expander		0.63			
In the regen per round trip					
Pockels cell (PC)	4	2			
Beam splitter (PBS2)		1.6345			
TiSa crystal (TS2)					5.08

Table 4.1: Length of dispersive materials used in the experimental set-up

correspond to the labels used in the design of the complete set-up as shown in appendix A, this table does not take the multi pass amplifier into account. The beam expander has not been included in this drawing of the design, but is has been used in the experiment. The oscillator creates a non dispersed pulse, due to its inner dispersion compensation performed by a prism pair. The

only dispersion induced in the oscillator originates from the last pass through the resonator cavity, and the elements responsible for the non-compensated dispersion are the TiSa crystal and the out couple mirror. A significant part of the material dispersion is generated by the regenerative amplifier as the light travels approximately 15 times up and down the regenerative amplifier and thus passing through these materials 30 times. To calculate the dispersion introduced by these materials, the corresponding Sellmeier equation has to be found, for which several sources are used. The main part of this information is found in [19] and others on the internet at the site of the manufacturer. The Sellmeier equations used, can be found in the Maple routine on the appended CD B. The Sellmeier equations represent the refractive index as a function of wavelength $n(\lambda)$, and therefore have to be rewritten to calculate the spectral phase disturbances by:

$$\frac{2\pi l_{mat} n(\lambda)}{\lambda} = \phi(\lambda) \tag{4.18}$$

And

$$\lambda = \frac{2\pi c}{\omega} \tag{4.19}$$

Using these equations the Sellmeier equations can be rewritten to spectral phase disturbance as function of material length l_{mat}, and frequency ω.
For calculation of the phase disturbance introduced by the compressor, $\phi(\omega)$ should be determined. Starting with determination of the path length through the compressor: The path length $\vec{P}$ is the sum of the two distances $\vec{ab}$ and $\vec{bc}$,

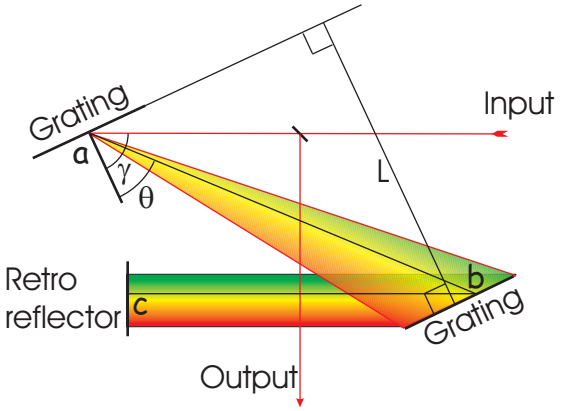

Figure 4.4: Schematic of compressor

$$\vec{ab} = \frac{L_g}{cos(\theta)}, \tag{4.20}$$

and

$$\vec{bc} = \vec{ab} \cdot cos(\gamma - \theta), \tag{4.21}$$

merging these two together according

$$\vec{P} = \vec{ab} + \vec{bc} = \frac{L_g}{cos(\theta)} \cdot (1 + cos(\gamma - \theta)) \tag{4.22}$$

Now the angles do depend on each other and on the wavelength, according to the grating equation for the first order diffraction:

$$sin(\gamma) + sin(\theta) = \frac{\lambda}{d} \tag{4.23}$$

where d is the groove spacing. The group delay is given by $\tau = P/c$. Since the diffracted angle is larger for longer wavelengths, a transform-limited pulse will emerge negatively chirped (short wavelengths precede longer wavelengths). The phase of the grating compressor can be derived in a number of ways owing to the arbitrary choice of an absolute phase and group delay (transit time). The most compact expression is given by Martinez *et al.*[16] originating from the equivalent optical path length:

$$P = \frac{\phi c}{\omega} = L_g cos(\theta) \tag{4.24}$$

Solving this expression for ϕ using the grating equation 4.23 gives the phase of a single pass through the compressor:

$$\phi(\omega) = \frac{\omega L_g}{c}\sqrt{1 - (\frac{2\pi c}{\omega d} - sin(\gamma))^2} \tag{4.25}$$

The design of the stretcher contains an extra telescope between the gratings. This telescope makes a projection of the first grating behind the second grating. As all the path lengths to this imaginary projection of the first grating are according the definition of an image of equal length. The distance between this imaginary grating and the second grating is then the same grating distance as is used for the compressor. Therefore the same equations hold for the stretcher as for the compressor, only the separation distance of the gratings is of opposite sign, and has to be taken from the projection of the first grating to the second grating as shown in figure 2.8.

4.2.2 Creation of the Maple model with the gathered data

Once all the Sellmeier equations of the materials and the corresponding material lengths are gathered, the spectral phase disturbance introduced by the material can be derived according to equation 4.15. For calculation of the spectral phase disturbance of the stretcher and compressor, equation 4.25 is used. The sum of these equations form an expression for the spectral phase of the entire set up. According to equation 4.17 the GVD, TOD, FOD and higher order dispersion can be determined by differentiation to the appropriate level. Note that the units of the GVD, TOD, FOD, etc. are normally expressed in respectively fs^2, fs^3, fs^4, etc. As the whole model derives these spectral phases in seconds, a conversion factor of respectively 10^{30}, 10^{45}, 10^{60}, etc. have to be applied. The model in Maple describes the dispersions as functions of the adjustable parameters. In that manner graphs of the dispersion can be plotted as function of grating distance (L_g), grating angle (γ) or any other important parameter of interest. See the appended CD B for the routine.

4.2.3 Find the optimal settings

The trigger to make another mathematical model of the system, were the poor results of the first two designs based on the available models. The whole set-up

had been built already, and only the compressor had to be set to an optimal configuration to cancel the dispersion. The only tunable parameters are the grating distance (L_g) and the grating angle (γ) of the compressor, therefore the first plots concern the dispersion of the whole set up as function of these parameters. Off course it is possible to produce other plots of the dispersion as function of other parameters like grating periodicity of the stretcher grating, but as these options are not available the number of free adjustable parameters are limited to the grating distance (L_g) and the grating angle (γ) of the compressor. The "dispersion landscape" provides much feeling about the response of the system on these settings, and makes it more easy to find the optimum in the lab. The "dispersion landscape" also showes the optimal settings for the compressor, and these settings appeared to be very accurate. The image of the "dispersion landscape" is shown in figure 4.5. It shows the three most important dispersion components GVD, TOD and FOD. A zero pane has been plotted as reference.

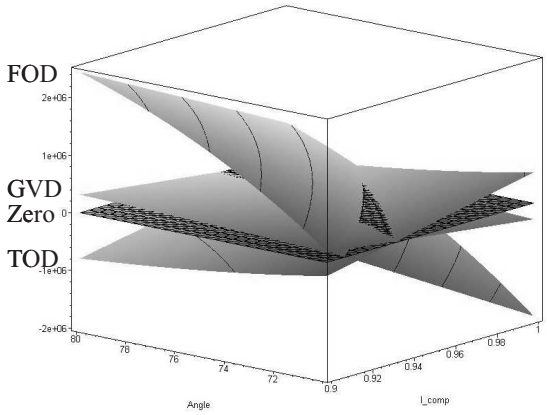

Figure 4.5: Dispersion landscape, the three orders of dispersion as function of L_g and γ

The "dispersion landscape" directly shows that it is not possible to cancel out all of the three dispersion components at the same settings. The optimal situation that can be realised is to cancel out only the GVD together with the TOD. To calculate this point, the two intersection lines of the GVD with the zero pane and the TOD with the zero pane, the crosspoint of these lines is than the optimal setting of the compressor. At this point the GVD as well as the TOD is then zero. The Maple routine also determines this point automatically. Another knob on the set-up is the knob to adjust the amount of round trips of the pulse through the regenerative amplifier. Although adjustment of the round trips through the regenerative amplifier affect the amplification efficiency, it is interesting to see what happens with the dispersion of the set-up when more material is introduced by more round trips through the regenerative amplifier. In first approximation, the regen round trips were set to 16 cycles, re-plotting the dispersion landscape for different values of regen round trips shows the following developments on the dispersion landscape. Note that the orientation of the plot has changed to a view from above. In this manner it is clearly visible at which points the dispersive components are equal to zero, as the intersection of the dispersion components with the hatched zero plane form a line. The hatched

triangle is the visible zero plane where all the dispersion components are smaller than zero. On the corners of this triangle two of the dispersion components are both equal to zero. Now the goal is to have all these corners merged into one point, making all the three dispersion components equal to zero, for one single compressor setting. By looking at the figure 4.6 it becomes clear that

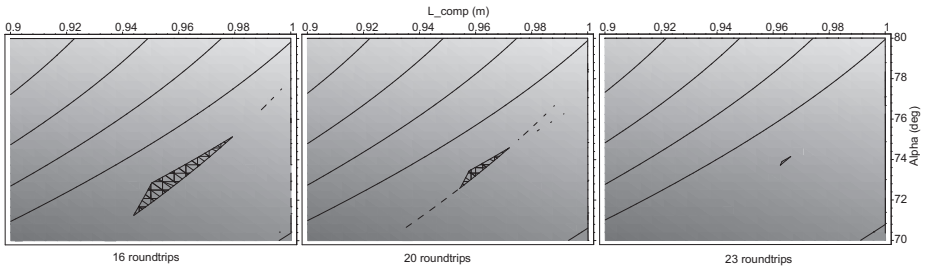

Figure 4.6: Changes observed in the 'dispersion' landscape due to additional round trips in the regen

introducing more material dispersion [21] by increasing the regen round trips, the amount of residual FOD develops to a minimum. The optimal number of cycles through the regenerative amplifier can be found by plotting the residual FOD as a function of regen round trips. As shown in figure 4.7, the GVD and the TOD are optimised to zero by adjustment of the set-up parameter to each of the derived points.

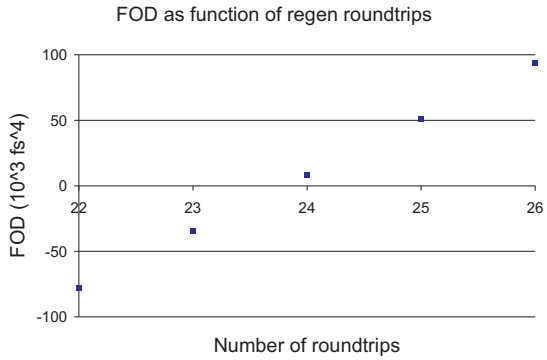

Figure 4.7: FOD as function of regen roundtrips

The optimal situation in the model predicts an optimal dispersion compensation for the present situation when the compressor parameters are set to $\gamma = 74.10\,\text{deg}$ and $L_g = 96.5cm$, with 24 cycles through the regenerative amplifier. An alternative method of compensation of higher order dispersion can be performed by adding extra material like BK7-glass or other materials. The following table shows the required amount of a single piece of additional material to compensate the FOD of the set-up. These numbers are based on 16 round trips in the regenerative amplifier while the optimal settings of the compressor were recalculated.
Although minor adjustments to the compressor settings have to be made to

Options for compensation of FOD by additional material	
Material	additional length (cm)
BK7	108.7
Sapphire	83.3
TGG	29.7
Calcite	140
DKDP	114

Table 4.2: Dispersive elements

compensate for FOD by additional materials, the amount of additional material is too large to implement it easily. The best option is an additional piece of 29.7 centimetres TGG to compensate FOD. It might be possible to insert a piece of additional material in the cavity of the regenerative amplifier, in which case only $\frac{1}{32}$nd of the material length would be sufficient. For implementation of such a piece of material in the regen cavity, it has to have an anti-reflection coating, or be placed at the Brewster angle but this last option will introduce large changes in the beam path. An advantage of placement of a second Brewster window in the could be the compensation of astigmatism in the cavity as measured in section 3.2.4. Some literature, like [11], describes correction of astigmatism by a Brewster window. But this has not been enquired to the full extend in this thesis.

CHAPTER 5

Comparison of mathematical models and experiments concerning dispersion

In this section the used mathematical models are compared with each other and with the experimental results. To compensate for the dispersion only two parameters, the grating angle (γ) and the grating distance (L_g), are adjustable for optimisation of the GVD and TOD. Compensation of FOD is only possible by insertion of additional materials. Adjustment of other parameters to tune the dispersion of the experiment is not easily performed as these parameters concern the properties of the materials used. Adjustments on the grating periodicity, for example, implicitly means replacement of these expensive devices. The results of the following items are discussed:

- Mathcad
- DOM (Disperse O Matic)
- Lab2
- Maple (Developed during this thesis)
- Experimental results

5.1 Comparison of the models in the most ideal situation

The optimal parameters for the set-up were found by the model in Maple, as the output of this model was the first one that worked well in the experimental set up. The parameters obtained from the Maple model are used in all the other mathematical models, in order to make a good comparison between the outputs of the different models. The parameters used are the material lengths and they are based on the optimal round trips through the regenerative amplifier for compensation of FOD as visualised in figure 4.7. This figure shows an optimal compensation of FOD for 24 round trips through the regenerative

amplifier. The input parameters of the mathematical models are presented in tables 5.1 and 5.2, presenting respectively the material lengths and the compressor settings.

The optimal compressor setting for this configuration derived with the model

Length of materials at 24 round trips	
Material	length (cm)
e-calcite	3.33
O-DKDP	96
BK7	90.135
o-sapphire	122.42
TGG	6

Table 5.1: Material lengths at 24 round trips

Stretcher settings	
Incident angle α	38°
perpendicular grating distance (L_g)	65.719 cm
Grating constant	1200 lines/mm

Table 5.2: Settings of stretcher

in Maple is displayed in table 5.3. Here the grating constant is an input parameter, as it is not easily adjustable. Comparison of the models used is performed by comparison of the residual GVD, TOD and FOD. In some of the used models the compressor settings are generated automatically, and therefore also taken into comparison. The next table shows these results of the used models. This table shows that the model in Maple and in Mathcad agree well, the compressor settings agree nicely and the GVD and TOD are in both cases zero. Only the FOD has the opposite sign. The output of the two remaining models present the same compressor settings, DOM is forced to these settings, and returns acceptable values for the dispersion (indicating that it is very close to an optimal setting). Lab 2 also indicates that these settings for the compressor are very close to the optimal ones, the indicator used for this result is the generated SHG-Frog trace in the program.

Note to Maple:
As the first good results in practice appeared after applying the configuration derived with the model written in Maple, the output of this model is used to compare the other models. This does not mean that the output of this model is the best of all, but since the results in practice were for the first time comparable to the outcome of this model it was more easy to apply these parameters on the other mathematical models to explore the failures made during the use of the other models. The pulse length is not well defined in this model, as only the GVD is used for estimation of the pulse length. Since the GVD is minimised, this value of GVD is only due to rounding errors.

Note to Lab2:
In this model the parameter g is not the perpendicular distance of the gratings,

Optimal compressor settings	
Incident angle (α)	74.12°
perpendicular grating distance (L_g)	96.53 cm
Grating constant	1500 lines/mm

Table 5.3: Optimal compressor settings derived by Maple

Modelled optimal compressor settings at 24 round trips						
Model	angle (°)	L_g (cm)	GVD fs^2	TOD fs^3	FOD fs^4	τ_p fs
Maple	74.12	96.53	$-3.5 \cdot 10^{-3}$	$1.4 \cdot 10^{-3}$	$1.04 \cdot 10^{4}$	25.00
Mathcad	73.50	96.06	$5.14 \cdot 10^{-5}$	$1.52 \cdot 10^{-4}$	$-5.72 \cdot 10^{4}$	27.46
DOM	74.12	96.53	-230.52	-215.62	$1.26 \cdot 10^{4}$	26.65
Lab2	74.08	96.52	-70.00	$4.00 \cdot 10^{3}$	$5.23 \cdot 10^{3}$	28.97

Table 5.4: Results of the used models for optimal compressor settings at 24 round trips

but the distance between the gratings. When aligned, the angle of the grating according to the optical axis of the stretcher is following the grating equation $\beta = asin((\lambda/d) - sin(\alpha)) = 20.14°$ resulting in a grating distance along the optical axis of 700 mm. As the model for the stretcher defines the distance between the grating surface and the focal point as g which is the half of the distances between the grating and the projection of the second grating. Therefore one has to use $g = 350$ mm and use two identical stretchers as the set-up consist of a four pass stretcher, while a stretcher has minimally 2 passes. Also

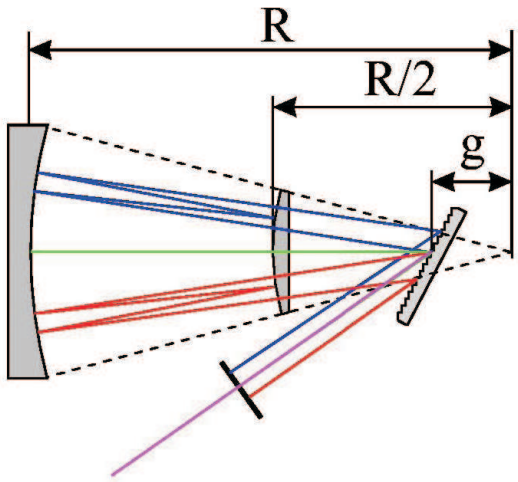

Figure 5.1: stretcher parameters in Lab2

the outcome of the compressor settings from the model in Lab2 are conform this approach, and have to be transformed to compare the results with the other mathematical models. Hereby the transmittance angle of the compressor grating is than $\beta_{comp} = 13.77°$, and the axial distance between the gratings of

$d = 99.4$ cm makes $L_g = 96.54$ cm of perpendicular distance. Lab2 optimises the compressor grating distance automatically, but not the grating angle. The two monitors (frog trace and pulse length) give sufficient feedback to optimise the grating angle manually, as the program takes less than a second to calculate the whole set-up it is easy to adjust this with the program in continuous running mode. The large residual dispersion numbers for GVD and TOD are not fully understood, it could be due to the fact that lab2 includes the effect that the compressor does not support the complete spectrum or due to rounding errors. But virtual enlargement of the gratings does not result in values around zero for the GVD or TOD. Also the response on minor adjustment does only reveal a minimal rounding error, not more than 5 fs^2 for the GVD. But these spectral boundaries agree well with the experiment as this effect is also visible and the tails of the spectrum miss the second grating of the compressor. Lab2 determines this spectral bandwidth by an infinitive small beam travelling

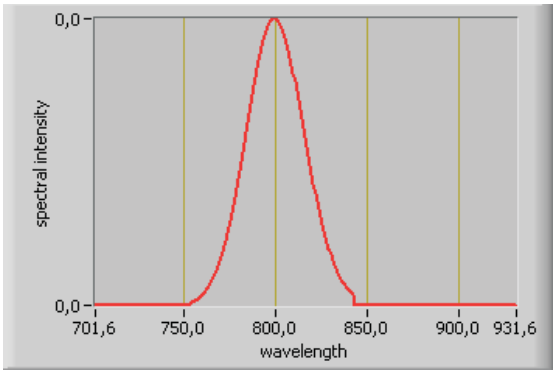

Figure 5.2: Modelled output spectrum of compressor

through the compressor. In the experiment the size of the beam is very large, making the edges of the spectrum less sharp and not measurable. But infra-red photographs show that a part of the spectrum misses the second grating of the compressor. Lab2 aligns the second grating to the central wavelength which is not the optimal manner to gather both spectral tails, as the projection on the second grating is not symmetrical due to the tilted angle of the second grating. Though this boundary results in minor asymmetric disturbances in the output spectrum of the model. Future designs of a compressor for higher energies have to avoid these effects, since the beam size increases to larger values as the power increases, and a larger fraction of light will not be projected on to the second grating.

Note to Mathcad:
As Mathcad has a built in optimisation routine, the angle and the grating distance of the compressor have changed to a minor degree. The model in Mathcad derives the results in a numerical manner. Although the model in Mathcad is based on the same input parameters, it generates a different output due to rounding processes for example. But fortunately the results agree very well with the other programs used. A nice feature of Mathcad is its option to gener-

ate a representation of the output pulse, as shown in the figure 5.3. One special

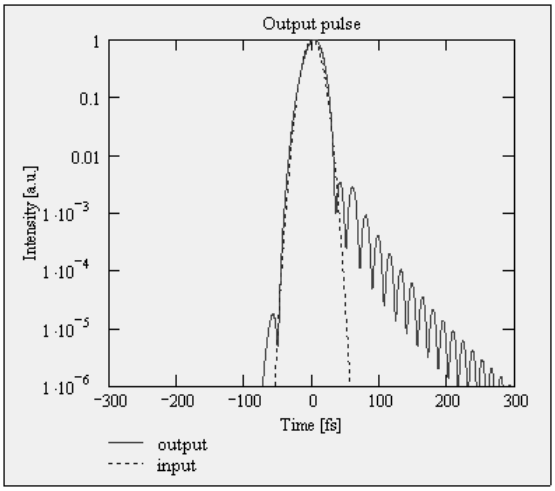

Figure 5.3: Theoretical intensity profile of the pulse

note has to be made concerning the use of the model in Mathcad. The names for the delay time "T" and second order dispersion "GDD" should be named GDD (group delay dispersion) and GVD (group velocity dispersion) respectively. But as these names are integrated into the whole model, the change of these names consumes too much effort for the same result.

Note to DOM:
The Disperse-O-Magic is a fast tool to check your system, the disadvantage is that no optimisation routine has been built in. But by moving the sliders gently, some optimal configurations can be derived, taking into account that the estimated output pulse length is only derived in the GVD, as the influences of higher order dispersion is not taken into account. This makes it possible to end up with several optimal configurations, as only one optimal configuration exist. The output here has not been optimised, therefore the GVD, TOD and FOD are again quite large, but still not destructively high. Manual optimisation easily drives these values to a minimum around zero with only tenths of a degree adjustments to the compressor grating angle and a few millimetres adjustments to the compressor grating distance. The conclusion can be drawn that DOM agrees well with the other models. A comment concerning this program is that GVD is called GDD, which is an incorrect name for GVD.

5.2 Comparison of the mathematical models to the experiment

In the experiment it is hard to approximate the theoretical optimum. In this case the models are mainly based on the practical experiment, but the round trips in the regenerative amplifier were not fixed yet, since at that moment of design of the models no fixed number of round trips had been chosen yet.

Now the regenerative amplifier has been optimised, restricting the variation of number of round trips. As this number of round trips does not agree with the optimal number of 24 round trips, the outcome of the mathematical models differ from the optimal result. Now the best solution has to be found for the experimental set-up with only 16 round trips through the regenerative amplifier. In this experimental case it is only possible to compensate the GVD and TOD, which is possible by adjustments of the compressor angle and compressor grating distance.

5.3 Determination for regen roundtrips

After fine tuning of the Regenerative amplifier to an optimal output power and stability the number of round trips can not be measured directly with the detector placed at its default position 'B', as in this manner the moment of injection is not detectable. For determination of the injection moment moment, the detector has to be installed in position 'A'. When the injection and extraction moments are obtained, it is possible to calculate the time the pulse is captured in the cavity. With the deterctor in position 'B', it is possible to measure duration time of one cycle. With these numbers it is possible to determine the number of roundtrips that the pulse makes through the regenerative amplifier. The images obtained at the scope at the corresponding positions of the detector are shown in figure 5.4. With the detector arranged at position 'A', the

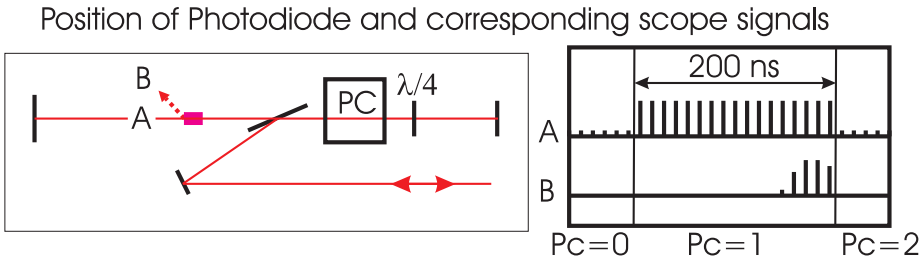

Figure 5.4: Positions of photo detector and their signals presented at the scope

moment of injection can be fine-tuned easily; as long as the amplitude of the last "spike" before the moment of injection is attenuated it is not correctly inserted into the regenerative amplifier. Measurements showed that it is only possible to fine-tune the moment of injection with help of a Grenouille trace of the re-compressed output pulse. This Grenouille trace shows the influence of the material dispersion when it is injected at a wrong moment. If this Grenouille trace is not available, then the optimal injection moment has to be determined with a detector placed at position 'A'.
Optimal settings for the regen showed a pulse capture time of 200 ns. The round trip time for this cavity of approximately 1.8 meters length should be around 12 ns, measurements showed that 7 round trips take 87 ns, which corresponds to a round trip time of 12.43 ns. Dividing the capture time through this measured round trip time gives 16 round trips through the regenerative amplifier. As the regenerative amplifier has been optimised for a stable output this number of round trips is used to determine the optimal settings for the compressor.

5.4 Modelling of the set-up according to the experimental settings

In order to make a nice comparison with the ideal case all of the available models are again used and compared with each other and the experiment.

Length of materials at 16 round trips	
Material	length (cm)
e-calcite	3.33
O-DKDP	64.00
BK7	61.063
o-sapphire	81.78
TGG	6.00

Table 5.5: Material lengths of the experimental set up

Compressor settings based on 16 round trips			
Model	angle (°)	L_g (cm)	τ_p fs
Maple	71.24	94.39	25.00
Mathcad	71.12	94.33	37.98
DOM	71.24	94.38	25.01
Lab2	71.26	94.39	29.32
Experiment	74.6 ±0.5	94.6 ±0.5	29 ±1

Table 5.6: Comparison the outcome of the mathematical models with the experimental results.

Note to Lab2:
The outcome of the Lab2 model has to be transformed to compare the results with the other mathematical models. Hereby the transmittance angle of the compressor grating is then $\beta_{comp} = 14.66°$, and the axial distance between the gratings of $d = 97.56\ cm$ makes $L_g = 94.39\ cm$ of perpendicular distance. Optimisation is again performed by manual adjustments of the grating angle, as the grating distance is automatically optimised, providing fast reliable results. An interesting feature of this package is the option to plot a SHG FROG trace. As the trace of a SHG FROG is identical to a Grenouille trace, which is the measurement method used in the experimental set-up. Therefore it is a nice tool to analyse the output in case it is not fully compensated. Images of these traces are used to compare the output of the set-up with the mathematical models 5.5.

Note to DOM:
The grating distance has been chosen to be the same as the Maple output, and small adjustments to the grating angle results in a low value for the GVD, and as the pulse duration is based on that figure, it is almost equal to the the input pulse duration of 25 fs.

5.5 Conclusions concerning the comparison between the mathematical models and the experimental results

The pulse duration shows large differences among the different models, the estimated pulse duration by Maple and DOM are only based on the GVD-term of the dispersion. As this value is controlled to an optimal value of zero, the pulse would have the same duration as the input pulse. Mathcad derives the pulse duration by taking the FWHM of a reconstructed envelope of the pulse that is based on the GVD, TOD, FOD and FifthOD. This sophisticated method generates, in contrast with the expectations, a pessimistic result of almost 38 fs. pulse duration. The reason for this difference can not be discovered, as all the equations used in the Mathcad routine agree the theory. Though this larger value of the pulse length is mainly induced by the FOD and the FifthOD. The results of Lab2 show the best agreement with the experimental values, concerning the pulse duration, the disadvantage is that it is not fully transparent how these numbers are generated. A nice option in Lab2 is to generate a Frog trace, this image can be compared with the trace from the experiment by a Grenouille, as the traces generated by a Grenouille or a Frog apparatus provide an identical interpretation of the pulse. The images are presented in figure 5.5. The shape of

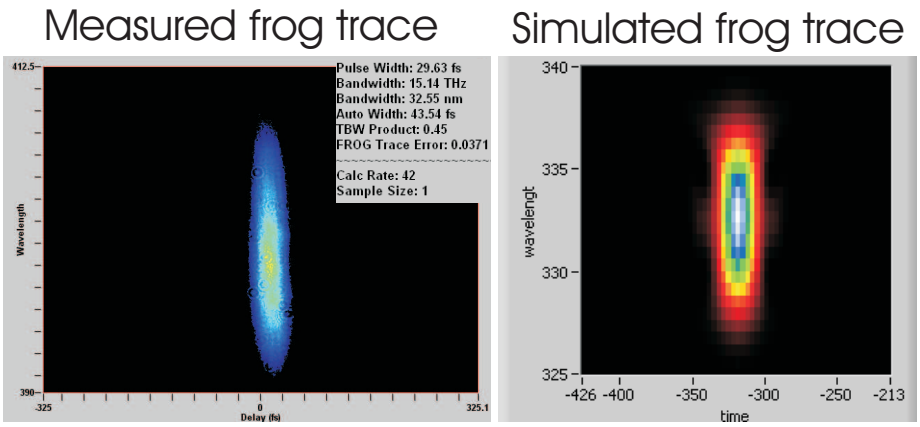

Figure 5.5: Measured Grenouille trace and derived Frog trace by Lab2

the images show large agreements, but the scale of the wavelength in the Lab2 model is not correct due to unknown reasons. But also the software used to measure the Grenouille trace of the experiments shows some errors during calibration of the wavelength axis. Therefore the measurements on the bandwidth could only be made by an external spectrometer. The scale of the measured wavelength in this graph agrees well with the spectrometer, even though the calibration was not successful. It can be concluded that the comparison of the experiment and the Lab2 model show large agreements, therefore Lab2 is a nice tool to predict the behaviour of the set up, including comparison of almost all the diagnostics that can be performed in the experiment.

The derived settings of the compressor show some differences with the settings

obtained in the experiment, especially the grating angle. These differences can largely be explained by misalignment of the stretcher. Adjustments to the input parameters of the Maple model, show that a stretcher angle of 39° instead of 38° result in compressor settings of: $L_{comp} = 0.94$ metres and an angle of 73.7°, whose are much closer to the values of the experiment. This, combined with a small red shift of the spectrum to 810nm, let the model in Maple come to a result of $L_{comp} = 0.94$ metres and an angle of 74.03°.

As the mathematical models derive the settings for the compressor very well, it is also interesting to explore the case when some parameters are changed to the set-up, and have the compressor settings be adjusted to re-compensate for the dispersion. This can be easily tested by adjustment of the number of round trips that the pulse is travelling through the regenerative amplifier. During this test the number of round trips through the regenerative amplifier are adjusted, and only the grating distance of the compressor is modified to optimise the output pulse length. A Grenouille is used to check the output pulse. To measure the small differences of grating distance a micrometer is used to measure the displacement of the second grating. To determine the absolute grating distance, the average distance differences between the measured points and the points derived by the Maple model have been added to the measured points, for easier to comparison of the mathematical model to the experiment. Other measurements show that this absolute grating distance is in the experiment slightly different from the distance derived by the model in Maple, which has been explained by minor alignment errors in the compressor. As the micrometer measures the translated distance along the optical axis, all measured points are converted to the perpendicular grating distance. In the model in Maple the grating angle is fixed to the optimal setting corresponding to 16 round trips, and only the grating distance is used to find the minimal GVD, which is basically the same action as performed in the experiment. The results are presented in figure 5.6. As this graph shows good agreements between the model in Maple and the

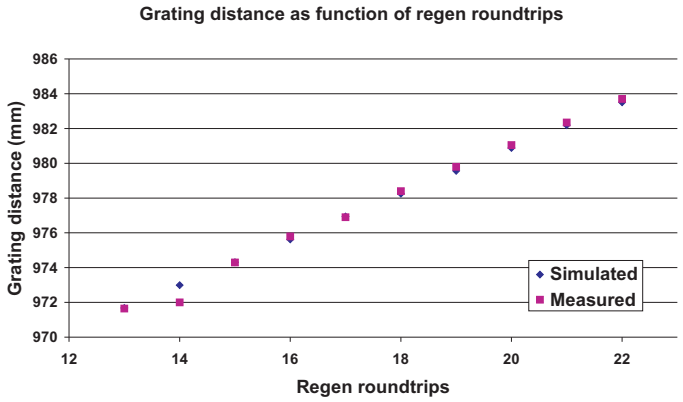

Figure 5.6: Grating distance as function of round trips in the regen, experimental results compared with the outcome of the mathematical model

experiment, it is a nice basis to predict the settings of the compressor for the two

last stages including the 4-pass and 2 pass amplifiers. Since the expectation is that the additional TiSa crystal introduced to the system will have only minor influence on the dispersion, only minor adjustments will presumably have to be made concerning the compressor settings. Therefore the idea is to calculate the differences in the compressor settings instead of the absolute settings as presented in the table 5.7.

Compressor settings for additional multi-pass amplifiers					
Parameter	optimal setting	4-pass		4- and 2-pass	
	for 16 passes	abs.	$\triangle$	abs.	$\triangle$
Angle (°)	71.24	71.47	0.23	71.57	0.33
L_{comp} (cm)	94.39	94.58	0.19	94.65	0.26

Table 5.7: Estimated compressor adjustments after installation of multi-pass amplifiers

These numbers are based on the parameters for the set-up with 16 passes through the regenerative amplifier, the two additional multi-pass amplifiers introduce only dispersion due to the TiSa crystal. The first 4-pass amplifier consist of an 18 mm TiSa crystal, and the last 2-pass amplifier is based on a 15 mm long TiSa crystal. This table reveals the expectation that additional dispersion introduced by the multi-pass amplifiers will have a minor influence on the compressor settings. But as the power of the pulse increases during these amplification stages, the beam size must increase as well to avoid damage to the optics. The increased beam size requires a larger second grating of the compressor, as it is already a bit too small for this purpose, displayed in figure 5.2 which is generated by the model of Lab2.

CHAPTER 6

Measurement of the output pulse

A Grenouille has been used to measure the final output of the experiment. In order to perform a good measurement on the pulse, the Grenouille has to be calibrated first. This section will discuss how the grenouille has been calibrated as described in [14], and finally the measured pulse shape of the output of the experiment is presented.

6.1 Calibration of the Grenouille

To calibrate the Grenouille a well defined pulse is used from the oscillator. The output of the oscillator is not completely dispersion free due to the last non-compensated pass through the crystal and the out-couple mirror of the oscillator itself. This compensation of dispersion is performed by prism compensation [22]. A thin film beam splitter and two mirrors are used to create a double pulse of this dispersion free pulse. Now this double pulse is put into the Grenouille for the actual calibration. Note that all the wavelengths must be halved, as a

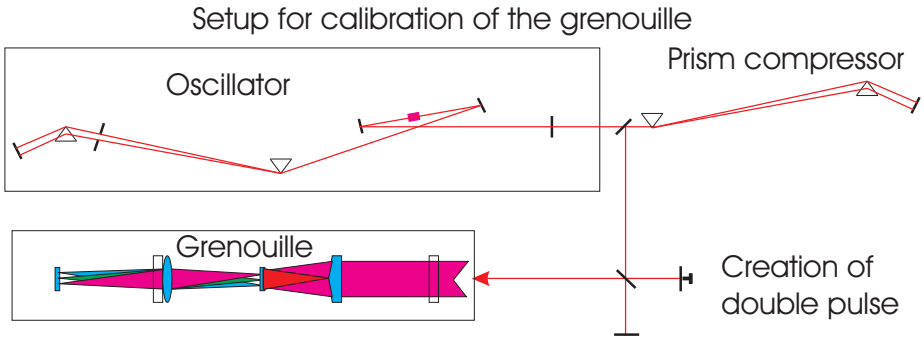

Figure 6.1: Setup for calibration of the Grenouille

frequency doubling crystal is used.
Two calibration measurements have been performed, and their Grenouille traces are shown in figure 6.2. The corresponding spectra, measured with an Ocean

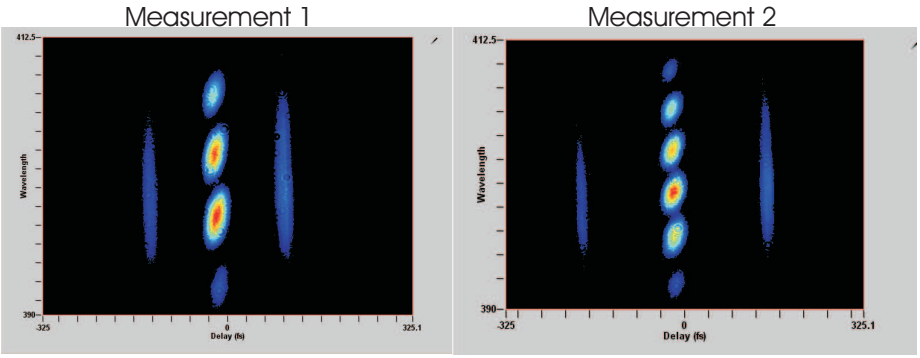

Figure 6.2: Grenouille traces of double pulse for calibration

optics USB2000 spectrometer, are presented in figure 6.3.

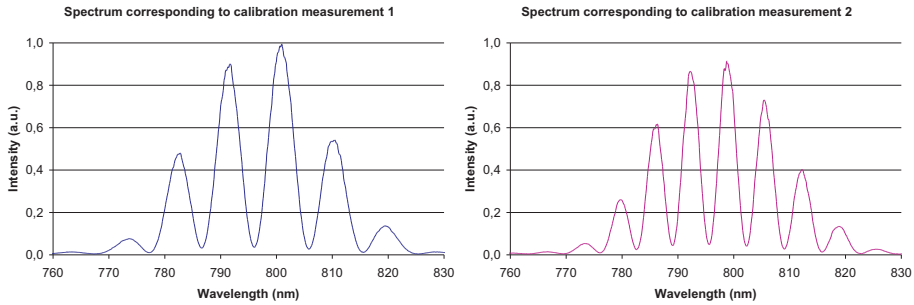

Figure 6.3: Measures spectra of double pulse, for calibration

Plotting the positions of the spectral peaks onto their pixel positions in the Grenouille trace in one graph, shown in figure 6.4, will produce a straight line. The slope of this line represents the value of the calibration parameter S_λ (nm/pixel) for the spectral axis of the program.
Along the time axis of the Grenouille trace, as shown in figure 6.2, three lobes are detected. The autocorrelation signal of two pulses generate a signal with three maxima. The first maxima, due to overlap of the first pulse with the second pulse, and in the central maxima is caused as both pulses overlap with each other (stronger signal), and the last maxima in the autocorrelator signal represents the overlap of the last with the first pulse, shown in figure 6.5.
For calibration of the time axis the separation time τ_{sep} must be determined, this can be derived from the average separation distance between the spectral lobes $\triangle\lambda$, according:

$$\tau_{sep} = \frac{\lambda_0^2}{\triangle\lambda \cdot c}, \tag{6.1}$$

where λ_0 is the centre wavelength and c the velocity of light. The used $\triangle\lambda$ in this experiment is the average separation distance between the maxima in the spectrum. For very broadband pulses, this is not the exact solution; the separation is constant for frequency, not wavelength. When the bandwidth is small, this effect is not significant. In the experiment this non-linearity has not

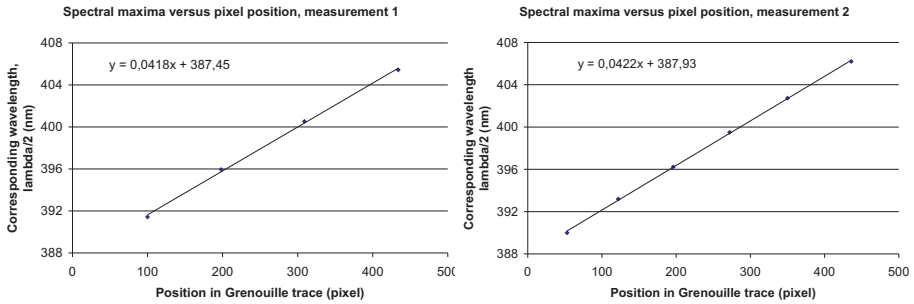

Figure 6.4: Wavelength of the spectral lobes mapped onto their position in the Grenouille trace

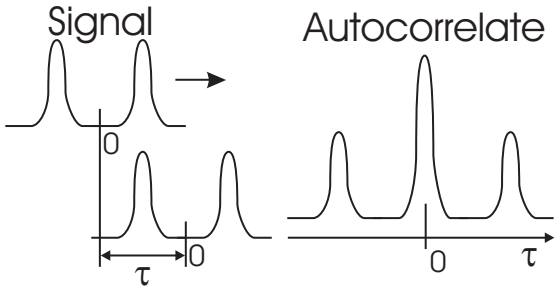

Figure 6.5: Representation of autocorrelaat of doublepulse

been observed, therefore this simplified method is used for calibration of the frequency axis. Once τ_{sep} is derived only the average separation distance of the three lobes in the time direction of the Grenouille trace $\triangle S_\tau$ (pixels) has to be measured, to determine the calibration value of the time axis S_t according:

$$S_t = \frac{\tau_{sep}}{\triangle S_\tau}, \tag{6.2}$$

The measured values for determination of the calibration and the derived calibration settings by this measurement are presented in table 6.1. The calibration

Measured values for determination of the calibration			
Calibration measurement	1	2	unit
Average $\triangle\lambda$	4.67	3.24	nm
τ_{sep}	457	658	fs
Average $\triangle S_\tau$	117	165	pixels
Derived calibration values			
S_t	3.905	3.989	fs/pixel
S_λ (Slope from fig. 6.4)	0.0418	0.0422	nm/pixel

Table 6.1: Measured and derived values for determination of the calibration values

values presented in table 6.1 for the time and wavelength axis, S_t and S_λ respectively, show only a few percent difference between outcome of the two calibration

measurements. This indicates that the calibration has been successful and the obtained values for the calibration are S_t=3.95±0.04 and S_λ=0.042±0.002.

6.2 Measured output pulse

Now the software of the Grenouille has been calibrated, it automatically determines the pulse duration. This measurement is performed on the output of the experiment. The pulse energy, obtained in earlier measurements before re-compression was approximately 3.5 mJ, and during that same measurement a energy of the pulse after re-compression of 2.5 mJ has been measured, this means that a compression efficiency of 71% has been reached. More detailed measurements of the grating efficiency can be found in the damage reports at the appended CD, appendix B. The repetition rate of the laser is 10 Hz, and according to the Grenouille trace, the pulse has a duration of 29.6 fs, as shown in the figure 6.6.

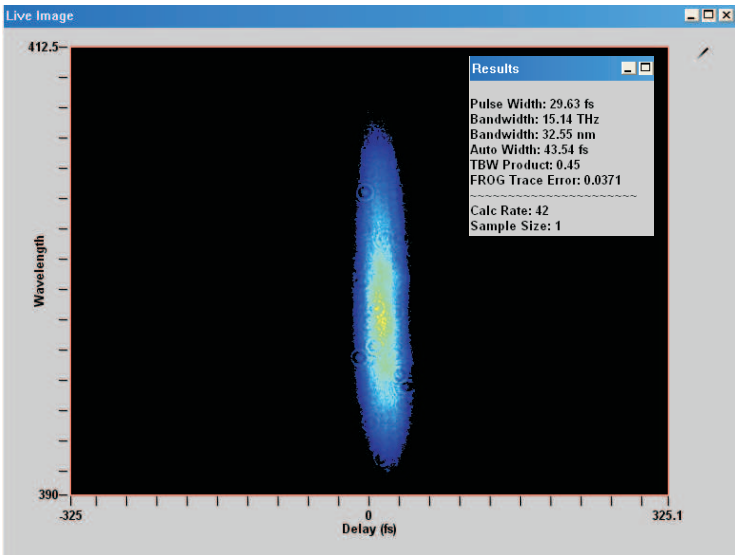

Figure 6.6: Output of experimental set up measured with Grenouille

CHAPTER 7

Conclusions

This report describes the design and construction of a regenerative amplifier and a grating compressor of a chirped pulse amplification laser as well as the characterisation of the output pulse. Also a mathematical model for the analysis of the dispersion of the set-up has been developed. The laser set-up generates a pulse of 29 fs with an energy of 2.5 mJ, which agrees with the expectations of the system.

7.1 Regenerative amplifier

The measured output pulse energy of 3.5 mJ of the regenerative amplifier agrees well with the expectations, based on theory. The experimental development of the beam waist has been compared with a theoretical model and agrees within the error margins, taking into account additional effects like thermal lensing.

7.2 Mathematical model for dispersion

Several models have been used and compared to calculate the dispersion in the system in order to re-compress the amplified stretched pulse coming out of the regenerative amplifier. The mathematical model in Mathcad has been improved by addition and correction of the Sellmeier equations used in this model. Another mathematical model has been written in Maple, and shows accurate values compared with the experimental settings. The option for producing a dispersion landscape provides the experimentalist a good picture of the dispersive behaviour of the experiment. Now the set-up can be modelled easily, providing information concerning adjustments to the settings of the compressor in order to adapt to changes in the experiment.

7.3 Re-compression of the pulse

The pulse has been re-compressed successfully, with help of the derived design by the mathematical models. The pulse has been re-compressed with an efficiency

of 71%. The spectrum of the pulse has been limited due to the finit dimensions of the second grating. The final output of the experiment is a 2.5 mJ pulse of 29 fs duration, starting from a 25 fs, 3nJ pulse from the oscillator. Thus the regenerative amplifier and the compressor have been successfully constructed and form a good basis for the further development of the 30 TW laser.

CHAPTER 8

Recommendations

Working with such a large laser system, reveals many points of attention. As long as the system runs every week, only the minor adjustments to the set up have to performed, this increases the reliability. The overall pointing stability can be improved by covering the whole set-up by boxes to avoid airflow. This also minimises the chance of damage to the optics due to dust particles. And by putting the laser into a box, the safety increases.

8.1 Regenerative amplifier

The output power of the regenerative amplifier is relatively stable due to the stabilisation effects of the regenerative amplifier, though fluctuations in the efficiency of the amplification can be observed by the manner how the energy of the pulse builds up in the cavity. These fluctuation can be caused by fluctuations of the pump laser. Mode-hopping of the pump laser could cause these effects,as a multi-mode pump laser is used instead of a single-mode pump laser. It is also possible that instabilities in the shot to shot power of this pump laser, generated by its power supply or degeneration of its flash-tubes, causes this effect. For a better understanding of these minor problems, this effect has to be examined to a further extend.

Long term measurements on the output power of the regenerative amplifier revealed a small increase in shot to shot power fluctuations. This could be readjusted easily, but the exact reason for this effect has not been found yet. For solving these problems it is recommended to monitor the output power of the pump laser over a long term. It could also be solved by adjustment of the cooling temperature of the TiSa crystal of the regenerative amplifier.

It has been demonstrated that the spectral behaviour of the regenerative amplifier can be manipulated by an etalon, manipulation of the spectrum has to be made in order to retrieve an as broad as possible spectrum around 800 nm, for creation of shorter pulses. A detailed investigation of the etalons influence should be performed in future.

8.2 Mathematical model for dispersion

The mathematical model of the dispersion of the set-up, does not include errors on the used input parameters. An additional feature would be to calculate margins on the generated compressor settings due to misalignment of the stretcher, as calculations have shown that this could be the cause of minor differences between the model and the experimental settings, shown in section 5.5.

8.3 Re-compression of the pulse

The bandwidth of the compressor is limited due to the size of the second grating, therefore a larger grating has to be installed. As a new grating has to be ordered, it is recommended to re-calculate the compressor settings for different grating periodicity of the compressor gratings. At this moment the compressor is set to an angle of 74°, which is near the limit of the acceptance angle of the grating. The advantage of this large angle, on the contrary, is that the optical power is smeared out over a larger surface of the grating. In this manner a smaller beam size can be applied without causing damage to the gratings. But, calculation with 16 round trips and a compressor based on 1400 lines/mm, instead of 1500 lines/mm, gratings showed optimal settings at L_g=1.07 meters and grating angle of 58°, which could have a better grating efficiency, although no significant losses have been measured on the gratings at the current set-up.

BIBLIOGRAPHY

[1] Geng, R.L.; Padamsee, H.; Seaman, A.; Shemelin, V.D., "World Record Accelerating Gradient Achieved in a Superconducting Niobium RF Cavity", PAC 2005. Proceedings of the , no.pp. 653 - 655, 16-20 May 2005

[2] R.Bingham, J.T. Medonca and P.K.Shukla. "Plasma based charged-particle accelerators." *plasmaphysics and controlled fusion*, 46 (2004) R1-R23.

[3] S. Backus *et al.*, "High power ultrafast lasers", Rev. Sci. Instrum., Vol 69, No 3, March 1998, .

[4] Arsen G. Khachatryan, "Trapping, compression, and acceleration of an electron bunch in the nonlinear laser wakefield", Physical Review E, vol. 65, 046504, 11 April 2002, Yerevan Physics Institute

[5] A.G. Khachatryan, F. A. van Goor, and K.-J. Boller, "Extremely short relativistic-electron-bunch generation in the laser wakefield via novel bunch injection scheme", Physical review special topics - Accelerators and Beams, Vol. 7, 121301, 6 December 2004, Department of Applied Science, University of Twente.

[6] M.J. van der Wiel *et al*, "Laser wakefield acceleration: the injection issue. Overview and latest results", Phil. Trans. R. Soc. A, rsta.2005.1731, Department of applied physics, Center For Plasma Physics and Radiation Technology, Eindhoven University of Technology.

[7] P. F. Moulton, "Spectroscopic and laser characteristics of Ti:Al_2O_3", J. Opt. Soc. Am. B., Vol. 3, No. 1, January 1986.

[8] C. Barty, T. Guo, C. Le Blanc, F. Raksi, C. Rose-Petruck, J. Squier, A.Tian, K. Wilson, V.Yakovlev, and K. Yamakawa, "Generation of 18-fs, multiterawatt pulses by regenerative pulse shaping and chirped-pulse amplification", Opt. Lett. vol. 21, 668 (1996).

[9] G. Cheriaux, *et al*, "Aberration-free stretcher design for ultrashort-pulse amplification", Opt. Lett. **21**, 414 (1996)

[10] A. Oeffner, U.S. patent 3,748,015 (1971).

[11] W. T. Silfast, "Laser Fundamentals", 2nd ed. ,Cambridge UK, Cambridge university press. (2004)

[12] Eugene Hecht, "Optics", 4 ed., San Francisco US. Addison Wesley.

[13] J.Squier, C.P.J.Barty, F. Salin, C. Le Blanc, S, Kane, "Use of Mismatched Grating Pairs in Chirped-pulse Amplification Systems", Appl. Opt. 37 (9), 1638 (1998)

[14] Rick trebino, "Frequency resolved optical gating: the measurement of ultrashort laser pulses", ISBN 1-4020-7066-7.

[15] A.Yariv, "Quantum electronics", 3rd. ed. (Wiley, New York, 1989).

[16] Martinez *et al*, "Negative group-velocity dispersion using refraction", J. Opt. Soc. Am. A., Vol. 1, No 10, pag. 1003, October 1984.

[17] P. W. Milonni, J. H. Eberly, "Lasers", (Wiley 1988), ISBN 0-471-62731-3.

[18] Prof. C. W. Siders, "Disperse-O-Matic", School of Optics / CREOL.

[19] M.Bass, "Handbook of optics", Optical society of America (McGraw-Hill New York, 1995).

[20] Dr. Ir. Ing F.A. van Goor. University of Twente.

[21] Florentina Rosca-Pruna, "Alignment of Diatomic Molecules Induced by Intense Laser Fields", ISBN 90-9015452-3, 2001, Amsterdam

[22] R. L. Fork, O. E. Martinez, and J. P. Gordon, "Negative dispersion using pairs of prisms" Opt. Lett. **9**, 150 (1984).

APPENDIX A

Schematic of experimental set up

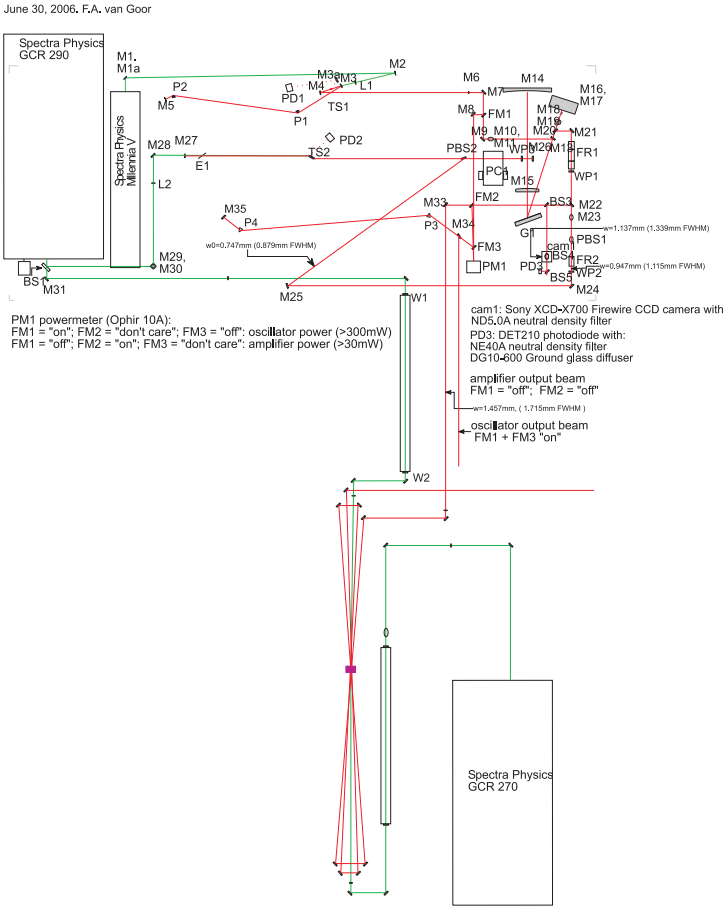

Figure A.1: Scematic of experimental set up

APPENDIX B
Additional CD

This CD contains:

- The used mathematical models, Maple, Lab2, Mathcad and DOM
- Calculations concerning the beam waist by matrix calculation
- Damage reports of the gratings
- A copy of this Report